MONOTONIC TENSILE AND FATIGUE TEST RESULTS INCLUDING OVERLOAD TESTS OF 1538MV AS-HOT ROLLED AND FORGED STEELS

AISI Iterations – 131 through 134

Z. Lopez and A. Fatemi

Department of Mechanical, Industrial, and
Manufacturing Engineering
The University of Toledo
Toledo, OH 43606

Prepared for:

The SMDI Bar Steel Applications Group

March 2012

Steel
Market Development
Institute

Steel Market Development Institute
2000 Town Center, Suite 320
Southfield, Michigan 48075
tel: 248-945-4777
fax: 248-352-1740
www.autosteel.org

TABLE OF CONTENTS

NOMENCLATURE

A_o, A_f	initial, final area	S	engineering stress
HB, HRB, HRC	Brinell, Rockwell B-Scale, Rockwell C-Scale Hardness number	YS, UYS, LYS, YS'	Monotonic yield, upper yield, lower yield, cyclic yield strength
b, c, n	fatigue strength, fatigue ductility, strain hardening exponent	YPE	yield point elongation
D_o, D_f	initial, final diameter	S_u	ultimate tensile strength
e	engineering strain	%EL	percent elongation
E, E'	monotonic, midlife cycle modulus of elasticity	%RA	percent reduction in area
K, K'	monotonic, cyclic strength coefficient	σ, σ_f, σ_f'	true stress, true fracture strength, fatigue strength coefficient
L_o, L_f	initial, final gage length	σ_a, σ_m, $\Delta\sigma$	stress amplitude, mean stress, stress range
$N_{50\%}$, $(N_f)_{10\%}$, $(N_f)_{50\%}$,	number of cycles to midlife, 10% load drop, 50% load drop,	ε_e, ε_p, ε	true elastic, plastic, total strain
$2N_f$	reversals to failure	ε_f, ε_f'	true fracture ductility, fatigue ductility coefficient
P_f, P_u	fracture, ultimate load	ε_a, ε_m, $\Delta\varepsilon$	strain amplitude, mean strain, strain range
R	strain ratio, neck radius	$\Delta\varepsilon_e$, $\Delta\varepsilon_p$	elastic, plastic strain range

NOMENCLATURE

$\sigma_{m,\,SC}$	small cycle mean stress	$\sigma_{a,\,SC}$	small cycle stress amplitude
$\sigma_{m,\,OL}$	overload cycle mean stress	$\sigma_{a,\,OL}$	overload cycle stress amplitude
$\varepsilon_{a,\,SC}$	small cycle strain amplitude	$(\Delta\varepsilon_p/2)_{SC}$	small cycle plastic strain amplitude,
$\varepsilon_{a,\,OL}$	overload cycle strain amplitude	$(\Delta\varepsilon_p/2)_{OL}$	overload plastic strain amplitude
$\varepsilon_{m,\,SC}$	small cycle mean strain	B, B_f	number of blocks in a periodic overload test, number of blocks to failure in a periodic overload test
N_{SC}, $N_{f,\,SC(eq)}$	number of small cycles in an overload block, calculated equivalent life of the small cycles in an overload test	$N_{f,\,OL}$	Constant amplitude life to failure at the strain amplitude used for the periodic overload cycle amplitude

UNIT CONVERSION TABLE

Measure	SI Unit	US Unit	from SI to US	from US to SI
Length	mm	in	1 mm = 0.03937 in	1 in = 25.4 mm
Area	mm^2	in^2	1 mm^2 = 0.00155 in^2	1 in^2 = 645.16 mm^2
Load	kN	klb	1kN = 0.2248 klb	1 klb = 4.448 kN
Stress	MPa	ksi	1 MPa = 0.14503 ksi	1 ksi = 6.895 MPa
Temperature	°C	°F	°C = (°F - 32)/1.8	°F = (°C * 1.8) + 32

In SI Unit:				
	1 kN = 10^3 N	1 Pa = 1 N/m^2	1 MPa = 10^6 Pa = 1 N/mm^2	1 Gpa = 10^9 Pa
In US Unit:				
	1 klb = 10^3 lb	1 psi = 1 lb/in^2	1 ksi = 10^3 psi	

SUMMARY

Monotonic tensile properties and fatigue behavior data were obtained for the 1538MV as-hot rolled and forged steels of iterations 131 and 133, respectively. The materials were provided by the American Iron and Steel Institute (AISI). For iterations 131 and 133, two tensile tests were performed to acquire the desired monotonic properties and eighteen strain-controlled fatigue tests were performed to obtain the fatigue life and cyclic deformation curves and properties. For iterations 132 and 134, periodic overload fatigue behavior and data were obtained from ten periodic overload fatigue tests for the 1538MV as-hot rolled and forged steels, respectively. The experimental procedure followed and results obtained are presented and discussed in this report.

I. EXPERIMENTAL PROGRAM

1.1 Material and Specimen Fabrication

1.1.1 Material

The SAE 1538MV as-hot rolled steel bar was provided by Gerdau MacSteel, Inc.. Microstructure of this material is shown in Figure 1. The 1538MV forged steel was provided in the form of crankshafts by General Motors. Microstructure of this material is shown in Figure 2.

1.1.2 Specimen

In this study, identical round specimens were used for monotonic and fatigue tests. The specimen configuration and dimensions are shown in Figure 3. This configuration deviates slightly from the specimen geometry recommended by ASTM Standard E606 [1]. The recommended specimens have uniform gage sections. The specimen geometry shown in Figure 3 differs by using a large secondary radius in the gage section to compensate for the slight stress concentration at the gage to grip section transition.

The SAE 1538MV Forged Steel was delivered to the University of Toledo in the form of round specimen blanks. The specimen blanks were machined from three sections (labeled B, C, and D) of seven General Motors crankshafts by Westmoreland Mechanical Testing and Research, Inc... Each section provided two specimen blanks as shown in Figure 4. The SAE 1538MV As-hot Rolled Steel was delivered to the University of Toledo in the form of square cross section specimen blanks.

Specimen machining was performed in the Mechanical, Industrial, and Manufacturing Engineering Machine Shop at the University of Toledo. The specimens were turned on a CNC lathe to achieve the tolerable dimensions specified on the specimen drawings.

The specimens were then polished prior to testing at the University of Toledo. A commercial round-specimen polishing machine was used to polish the specimen gage section. Three different grits of aluminum oxide lapping film 30 μm, 12 μm, and 3 μm were used. Polishing marks coincided with the longitudinal direction of the specimen. The polished surfaces were carefully examined under magnification to ensure complete removal of machine marks within the test section.

1.2 Testing Equipment

1.2.1 Apparatus

An MTS closed-loop servo-controlled hydraulic axial load frame in conjunction with an INSTRON 8800 Fast-Track digital servo-controller was used to conduct the tests. The load cell used had a capacity of 100 kN. Hydraulically operated grips using wedge inserts with a circular cavity were employed to secure the specimens' ends in series with the load cell.

Total strain was controlled using an extensometer rated as ASTM class B2 [2]. The calibration of the extensometer was verified using displacement apparatus containing a micrometer barrel in divisions of 0.0001 in. The extensometer had a gage length of 0.30 in. and was capable of measuring strains up to 15 %.

In order to protect the specimens' surface from the knife-edges of the extensometer, ASTM Standard E606 recommends the use of transparent tape or epoxy to

'cushion' the attachment. For this study, it was found that application of transparent tape allowed for more consistency of the material thickness between the knife edge and the specimen. Therefore, transparent tape was considered to be the best protection. The tests were performed using three layers of transparent tape.

1.2.2 Alignment

Significant effort was put forth to align the load train (load cell, grips, specimen, and actuator). Misalignment can result from both tilt and offset between the central lines of the load train components. In order to align the machine, a round strain-gage bar was used. The Strain-gage bar has two arrays of four strain gages per array with one array arranged at the upper and lower ends of the uniform gage section. This was done in accordance with ASTM Standard E1012 [3].

1.3 Test Methods and Procedures

1.3.1 Monotonic tension tests

Monotonic tests in this study were performed using test methods specified by ASTM Standard E8 [4]. Two specimens were used to obtain the monotonic properties of iterations 131/132 and 133/134.

In order to protect the extensometer, strain control was used only up to 10% strain, until the point of ultimate tensile strength had been crossed. After this point, displacement control was used until fracture. INSTRON Bluehill software was used for the monotonic tests. For the elastic and initial yield region (0% to 1% strain) a strain rate of 0.0025 mm/mm/min was chosen. This strain rate was about one half of the maximum allowable rate specified by ASTM Standard E8 for the initial yield region. After the

strain reached 1% a strain rate of 0.005 mm/mm/min was used up until the extensometer was removed. This strain rate was ten percent of the maximum allowable rate specified by ASTM Standard E8 for the region after yielding. After the extensometer was removed, a displacement rate of 0.2 mm/min was used.

After the tension tests were concluded, the broken specimens were carefully reassembled. The final gage lengths of the fractured specimens were measured with a Vernier caliper having divisions of 0.001 in. Using an optical comparator with 10X magnification and divisions of 0.001 in, the final diameter and neck radius were measured. It should be noted that prior to the test, the initial diameter was measured with this same instrument.

1.3.2 Constant amplitude fatigue tests

All constant amplitude fatigue tests in this study were performed according to ASTM Standard E606. It is recommended by this standard that at least 10 specimens be used to generate the fatigue properties. 18 specimens at 7 different strain amplitudes ranging from 0.175% to 2.000% were utilized for iterations 131/132 and 133/134. INSTRON SAX software was used in all strain-controlled tests. During each strain-controlled test, the total strain was recorded using the extensometer output. Test data were automatically recorded throughout each test.

There were two control modes used for these tests. Strain control was used in all tests with plastic deformation. For one of the elastic tests from iteration 133/134, strain control was used initially to determine the stabilized load, and then load control was used for the remainder of the test. For the rest of the elastic tests, load control was used throughout. The reason for the change in control mode was due to the frequency

limitation on the extensometer. For the strain-controlled tests, the applied frequencies ranged from 0.2 Hz to 1.4 Hz for iteration 131/132 and from 0.3 Hz to 2.0 Hz for iteration 133/134, in order to keep a strain rate about 0.02 in/in/sec. For the load-controlled tests, load waveforms with frequencies of up to 20 Hz for iteration 131 and 25 Hz for iteration 133/134 were used in order to shorten the overall test duration. All tests were conducted using a triangular waveform.

1.3.3 Periodic overload fatigue tests

The overload tests were conducted to investigate the effects of periodic overloads on the fatigue life of smaller subsequent cycles. For iteration 131/132, 10 specimens were tested at 4 different strain amplitudes. For iteration 133/134, 10 specimens were tested at 5 different strain amplitudes. All of the overload tests were performed in load-control after the initial pre-cycles. The periodic overload tests were performed with INSTRON WAVERUNNER software. Test data were automatically recorded throughout each test.

The input signal consisted of a periodic fully reversed overload of the type shown in Figure 22. The load history in these tests consisted of repeated blocks made up of one fully-reversed overload cycle followed by a group of smaller constant amplitude cycles having the same maximum stress as the overload cycle. The overload cycles were applied at frequent intervals to maintain a larger effective strain range resulting in the subsequent cycles being fully effective.

With this overload history, as the large cycles become more frequent, the fraction of the total damage done by them increase and that done by the small cycles decrease. The fully reversed strain amplitude for the overload cycle was about 0.4% and corresponded to about 10^4 cycles to failure. The number of small cycles per block, N_{sc},

were adjusted so that they cause 80% to 90% of the damage per block. Small cycle strain levels were selected at or below the run out level of the constant amplitude tests. Small cycle strain amplitudes were used from 0.075% to 0.200% for iteration 131, and from 0.060% to 0.175% for iteration 133/134. The number of small cycles per overload cycle ranged between 40 and 2000 for both iterations.

For the load-controlled tests, calculations were performed based on equation 6 in order to arrive at the steady state stress amplitudes for the desired strain amplitudes. Due to the transient response of the material, the calculated loads would result in a lower than expected strain amplitude throughout the test. In order to reduce cyclic transient behavior, 1000 strain-control pre-cycles were applied at the periodic overload strain level of 0.4%. After completion of these initial cycles the second portion of the test was started using the previously mentioned periodic overload history.

II. EXPERIMENTAL RESULTS AND ANALYSIS

2.1 Microstructural Data

The chemistry of both materials is presented in Table 1. Figures 1 and 2 show magnified views of the microstructure of the 1538MV as-hot rolled and forged steels, respectively. The microstructural data for these steels was provided by Gerdau MacSteel.

2.2 Monotonic Deformation Behavior

The properties determined from monotonic tests were the following: modulus of elasticity (E), yield strength (YS), ultimate tensile strength (S_u), percent elongation (%EL), percent reduction in area (%RA), true fracture strength (σ_f), true fracture ductility (ε_f), strength coefficient (K), and strain hardening exponent (n).

True stress (σ), true strain (ε), and true plastic strain (ε_p) were calculated from engineering stress (S) and engineering strain (e), according to the following relationships which are based on constant volume assumption:

$$\sigma = S(1+e) \tag{1a}$$

$$\varepsilon = \ln(1+e) \tag{1b}$$

$$\varepsilon_p = \varepsilon - \varepsilon_e = \varepsilon - \frac{\sigma}{E} \tag{1c}$$

The true stress (σ) - true strain (ε) plot is often represented by the Ramberg-Osgood equation:

$$\varepsilon = \varepsilon_e + \varepsilon_p = \frac{\sigma}{E} + \left(\frac{\sigma}{K}\right)^{\frac{1}{n}} \tag{2}$$

The strength coefficient, K, and strain hardening exponent, n, are the intercept and slope of the best line fit to true stress (σ) versus true plastic strain (ε_p) data in log-log scale:

$$\sigma = K\left(\varepsilon_p\right)^n \tag{3}$$

In accordance with ASTM Standard E739 [5], when performing the least squares fit, the true plastic strain (ε_p) was the independent variable and the true stress (σ) was the dependent variable. These plots for the two tests conducted for iterations 131 and 133 are shown in Figures 5(a) and (b), respectively. To generate the K and n values, the range of data used in this figure was chosen according to the definition of discontinuous yielding specified in ASTM Standard E646 [6]. Therefore, the valid data range occurred between the end of yield point extension and the strain at maximum load.

The true fracture strength was corrected for necking according to the Bridgman correction factor [7]:

$$\sigma_f = \frac{\frac{P_f}{A_f}}{\left[1+\frac{4R}{D_f}\right]\ln\left[1+\frac{D_f}{4R}\right]} \tag{4}$$

where P_f is load at fracture, R is the neck radius, and D_f is the diameter at fracture.

The true fracture ductility, ε_f, was calculated from the relationship based on constant volume:

$$\varepsilon_f = \ln\left(\frac{A_o}{A_f}\right) = \ln\left(\frac{1}{1-RA}\right) \tag{5}$$

where A_f is the cross-sectional area at fracture, A_o is the original cross-sectional area, and RA is the reduction in area.

The monotonic stress-strain curves for iterations 131 and 133 are shown in Figures 6(a) and (b), respectively. As can be seen from both figures, the two curves are close to each other. In Figure 7, the monotonic stress-strain curves for iterations 131 and 133 are superimposed. As shown in this figure, the stress-strain curves of iteration 131 are above those of iteration 133. Refer to Table A-1 for a summary of the monotonic test results from iterations 131 and 133, respectively.

2.3 Cyclic Deformation Behavior

2.3.1 Transient cyclic response

Transient cyclic response describes the process of cyclic-induced change in deformation resistance of a material. Data obtained from constant amplitude strain-controlled fatigue tests were used to determine this response. Plots of stress amplitude variation versus applied number of cycles can indicate the degree of transient cyclic softening/hardening. Also, these plots show when cyclic stabilization occurs. Composite plots of the transient cyclic response studied are shown in Figures A-1 and A-2. The transient response is normalized on the rectangular plot in Figures A-1(a) and (b) for iterations 131 and 133, respectively, while a semi-log plot is shown in Figures A-2(a) and (b) for iterations 131 and 133, respectively. Even though multiple tests were conducted at each strain amplitude, data from one test at each strain amplitude tested is shown in these plots.

2.3.2 Steady-state cyclic deformation

Another cyclic behavior of interest was the steady state or stable response. Data obtained from constant amplitude strain-controlled fatigue tests were also used to determine this response. The properties determined from the steady-state hysteresis loops were the following: cyclic modulus of elasticity (E'), cyclic strength coefficient (K'), cyclic strain hardening exponent (n'), and cyclic yield strength (YS'). Half-life (midlife) hysteresis loops and data were used to obtain the stable cyclic properties.

Similar to monotonic behavior, the cyclic true stress-strain behavior can be characterized by the Ramberg-Osgood type equation:

$$\frac{\Delta \varepsilon}{2} = \frac{\Delta \varepsilon_e}{2} + \frac{\Delta \varepsilon_p}{2} = \frac{\Delta \sigma}{2E} + \left(\frac{\Delta \sigma}{2K'} \right)^{\frac{1}{n'}} \tag{6}$$

It should be noted that in Equation 6 and the other equations that follow, E is the average modulus of elasticity that was calculated from the monotonic tests.

The cyclic strength coefficient, K', and cyclic strain hardening exponent, n', are the intercept and slope of the best line fit to true stress amplitude ($\Delta\sigma/2$) versus true plastic strain amplitude ($\Delta\varepsilon_p/2$) data in log-log scale:

$$\frac{\Delta \sigma}{2} = K' \left(\frac{\Delta \varepsilon_p}{2} \right)^{n'} \tag{7}$$

In accordance with ASTM Standard E739 [5], when performing the least squares fit, the true plastic strain amplitude ($\Delta\varepsilon_p/2$) was the independent variable and the stress amplitude ($\Delta\sigma/2$) was the dependent variable. The true plastic strain amplitude was calculated by the following equation:

$$\frac{\Delta \varepsilon_p}{2} = \frac{\Delta \varepsilon}{2} - \frac{\Delta \sigma}{2E} \tag{8}$$

This plot is shown in Figures 8(a) and (b) for iterations 131 and 133, respectively. To generate the K' and n' values, the range of data used in these figures was chosen for

$$\left[\frac{\Delta \varepsilon_p}{2}\right]_{calculated} \geq 0.0004 \text{ in/in.}$$

The cyclic stress-strain curve reflects the resistance of a material to cyclic deformation and can be vastly different from the monotonic stress-strain curve. The cyclic stress-strain curves for iterations 131 and 133 are shown in Figures 9(a) and (b), respectively. The cyclic stress-strain curves for both iterations are superimposed in Figure 10. In Figures 11 and 12, monotonic and cyclic curves are superimposed for iterations 131 and 133, respectively. As can be seen in these figures, both materials cyclically harden. A composite plot of the steady-state (midlife) hysteresis loops is shown in Figures A-3(a) and (b) for iterations 131 and 133, respectively. Even though multiple tests were conducted at each strain amplitude, the stable loops from only one test at each strain amplitude are shown in these plots.

2.4 Constant Amplitude Fatigue Behavior

Constant amplitude strain-controlled fatigue tests were performed to determine the strain-life curve. The following equation relates the true strain amplitude to the fatigue life:

$$\frac{\Delta \varepsilon}{2} = \frac{\Delta \varepsilon_e}{2} + \frac{\Delta \varepsilon_p}{2} = \frac{\sigma_f'}{E}(2N_f)^b + \varepsilon_f'(2N_f)^c \tag{9}$$

where σ_f' is the fatigue strength coefficient, b is the fatigue strength exponent, ε_f' is the fatigue ductility coefficient, c is the fatigue ductility exponent, E is the monotonic modulus of elasticity, and $2N_f$ is the number of reversals to failure.

The fatigue strength coefficient, σ_f', and fatigue strength exponent, b, are the intercept and slope of the best line fit to true stress amplitude ($\Delta\sigma/2$) versus reversals to failure ($2N_f$) data in log-log scale:

$$\frac{\Delta\sigma}{2} = \sigma_f' (2N_f)^b \tag{10}$$

In accordance with ASTM Standard E739, when performing the least squares fit, the stress amplitude ($\Delta\sigma/2$) was the independent variable and the reversals to failure ($2N_f$) was the dependent variable. This plot is shown in Figures 13(a) and (b) for iterations 131 and 133, respectively. Superimposed data from both iterations is shown in Figure 14. To generate the σ_f' and b values, all data, with the exception of the run-out tests, in the stress-life figure were used.

The fatigue ductility coefficient, ε_f', and fatigue ductility exponent, c, are the intercept and slope of the best line fit to calculated true plastic strain amplitude ($\Delta\varepsilon_p/2$) versus reversals to failure ($2N_f$) data in log-log scale:

$$\left(\frac{\Delta\varepsilon_p}{2}\right)_{calculated} = \varepsilon_f' (2N_f)^c \tag{11}$$

In accordance with ASTM Standard E739, when performing the least squares fit, the calculated true plastic strain amplitude ($\Delta\varepsilon_p/2$) was the independent variable and the reversals to failure ($2N_f$) was the dependent variable. The calculated true plastic strain amplitude was determined from Equation 8. This plot is shown in Figures 15(a) and (b)

for iterations 131 and 133, respectively. Superimposed data from both iterations is shown in Figure 16. To generate the ε_f' and c values, the range of data used in these figures was chosen for $\left[\frac{\Delta\varepsilon_p}{2}\right]_{calculated} \geq 0.0004$ in/in.

The true strain amplitude versus reversals to failure plot is shown in Figures 17(a) and (b) for iterations 131 and 133, respectively. This plot displays the strain-life curve (Eqn. 9), the elastic strain portion (Eqn. 10), the plastic strain portion (Eqn. 11), and superimposed fatigue data. The strain-life curves for both iterations are superimposed in Figure 18. As can be seen from this figure, iteration 131 has inferior fatigue performance at short life (i.e. less than 1E+4 reversals to failure) but superior fatigue performance at long life (i.e. greater than 1E+4 reversals to failure) compared to iteration 133. A summary of the cyclic properties for both iterations is provided in Table 2. Tables A-2 and A-3 provide a summary of the fatigue test results for iterations 131 and 133, respectively.

It was mentioned in Section 1.1.2 that the specimens of iteration 133 were machined from three sections of a crankshaft. In Figure 19, strain-life fatigue data from these sections are superimposed in the true strain amplitude versus reversals to failure plot and labeled B, C, and D. At each strain amplitude, specimens from different sections of the crankshaft were tested. As can be seen from this figure, there is no difference in the fatigue behavior between specimens of sections B, C, and D.

A parameter often used to characterize fatigue behavior at stress concentrations, such as at the root of a notch, is Neuber parameter [7]. Neuber's stress range is given by:

$$\sqrt{(\Delta\varepsilon)(\Delta\sigma)E} = 2\sqrt{(\sigma_f')^2(2N_f)^{2b} + \sigma_f'\varepsilon_f'E(2N_f)^{b+c}} \qquad (12)$$

A plot of Neuber stress range versus reversals to failure is shown in Figures 20(a) and (b) for iterations 131 and 133, respectively. The Neuber curve based on Eqn. 12 and superimposed fatigue data for each material is displayed in these figures. In Figure 21, the Neuber curves and fatigue data of both iterations are superimposed. The same trends that were shown in Figure 18 can be seen in this figure.

2.5 Periodic Overload Fatigue Behavior

Periodic Overload fatigue tests were performed to determine the effective strain-life curve. The effective strain-life curve is plotted using the strain amplitude of the small cycles in the overload block and the calculated equivalent life. The equivalent fatigue life for the smaller cycles was obtained using the linear damage rule:

$$\frac{N_{OL}}{N_{f,OL}} + \frac{N_{SC}}{N_{f,SC(eq)}} = 1 \qquad (13)$$

where N_{OL} is the number of overload cycles in a periodic overload test, $N_{f,OL}$ is the number of cycles to failure if only overloads were applied in a test, N_{SC} is the number of smaller cycles in a periodic overload test, and $N_{f,SC(eq)}$ is the computed equivalent fatigue life for the smaller cycles.

The linear damage rule was also used to calculate the cumulative damage of the overload cycles, D_{OL}, as

$$\frac{N_{OL}}{N_{f,OL}} = D_{OL} \qquad (14)$$

Figures 23(a) and (b) show the effective strain-life data superimposed on the constant amplitude strain life plot for iterations 131 and 133, respectively. This data for both

iterations is superimposed in Figure 24. Tables A-4 and A-5 present a summary of the periodic overload test results for iterations 131 and 133, respectively.

It was mentioned in Section 1.1.2 that the specimens of iteration 133 were machined from three sections of a crankshaft. In Figure 25, periodic overload fatigue data from these sections are superimposed in the true strain amplitude versus reversals to failure plot and labeled B, C, and D. At each strain amplitude, specimens from different sections of the crankshaft were tested. As can be seen from this figure, there is no difference in the periodic overload fatigue behavior between specimens of sections B, C, and D.

A plot of the SWT parameter for both the constant amplitude and overload data provides another method of comparison between the two sets of data, where the mean stress present in the small cycles is taken into account. The SWT parameter is given by

$$\sigma_{\max}\varepsilon_a = \frac{1}{E}[(\sigma_f')^2(2N_f)^{2b} + \sigma_f'\varepsilon_f' E(2N_f)^{b+c}] \qquad (15)$$

where $\sigma_{\max} = \sigma_m + \sigma_a$. The SWT plot is shown in Figures 26(a) and (b) for iterations 131 and 133, respectively. This data for both materials is superimposed in Figure 27. As in Figure 24, the overload data and effective strain-life curve diverged from the constant amplitude curve.

Table 2: Summary of the Mechanical Properties

Microstructural Data	3M74155	3M73212	4M73828	4M73833	4M73835	4M73836
	Average					
ASTM grain size number (MAG=500X):						
First longitudinal direction (L-T)						
Inclusion rating number (MAG=100x): (Provided by Macsteel Company)						
Type A (sulfide type), thin & heavy series	2.50	2.25	2.25	2.25	2.25	2.25
Type B (alumina type), thin & heavy series	0.25	0.25	0.25	0.25	0.25	0.50
Type C (silicate type), thin & heavy series	none	none	none	none	none	none
Type D (globular type), thin & heavy series	0.50	0.50	0.75	0.50	0.50	0.50
Hardness:						
Brinell (HB)(measured)						
the first longitudinal direction	285.0	279.7	274.3	285.0	269.0	274.3
Transverse direction	-	-	-	-	-	-
Rockwell B-scale (HRB)						
The first longitudinal direction	-	-	-	-	-	-
Transverse direction	-	-	-	-	-	-
Rockwell C-scale (HRC)(converted)						
The first longitudinal direction	-	-	-	-	-	-
Transverse direction	-	-	-	-	-	-
Microstructure type:						
The first longitudinal direction	-	-	-	-	-	-
Transverse direction	-	-	-	-	-	-

Monotonic Properties	IT 131	IT 133	IT 131			IT 133		
	Average		Range					
Modulus of elasticity, E, GPa (ksi):	193.2	193.5	201.5	-	184.8	196.0	-	191.0
Yield strength (0.2% offset), YS , MPa (ksi):	650.3	627.9	660.5	-	640.0	626.8	-	629.0
Upper yield strength UYS, MPa (ksi):	-	-						
Lower yield strength LYS, MPa (ksi):	-	-						
Yield point elongation, YPE (%):	-	-						
Ultimate strength, S_u , MPa (ksi):	973.4	943.2	958.3	-	988.4	942.1	-	944.4
Percent elongation, %EL (%):	24.9%	26.7%	27.4%	-	22.4%	23.0%	-	30.4%
Percent reduction in area, %RA (%):	28.3%	36.4%	26.3%	-	30.3%	37.4%	-	35.4%
Strength coefficient, K , MPa (ksi):	1,480.2	1,445.5	1,486.2	-	1,474.3	1,469.4	-	1,421.7
Strain hardening exponent, n:	0.1422	0.1446	0.1418	-	0.1425	0.1489	-	0.1403
True fracture strength, σ_f, MPa (ksi):	1038.7	1069.8	1029.6	-	1047.9	1043.6	-	1096.1
True fracture ductility, ε_f (%):	33.3%	45.2%	30.5%	-	36.1%	46.8%	-	43.6%
Cyclic Properties	**Average**		**Range**					
Cyclic modulus of elasticity, E' , GPa (ksi):	193.9	190.2	203.3	-	182.6	204.8	-	179.2
Fatigue strength coefficient, σ_f' , MPa (ksi):	1,354.7	1,550.3						
Fatigue strength exponent, b:	-0.0776	-0.0965						
Fatigue ductility coefficient, ε_f' :	0.801	1.846						
Fatigue ductility exponent, c:	-0.6875	-0.7617						
Cyclic strength coefficient, K' , MPa (ksi):	1,447.1	1,416.5						
Cyclic strain hardening exponent, n':	0.1210	0.1247						
Cyclic yield strength, YS', MPa (ksi)	682.4	652.6						
Fatigue Limit (defined at 10^6 cycles), Mpa (ksi)	439.1	382.3						

Table 1: Chemical Composition of 1538 MV Forged Steel (Courtesy of Gerdau-MacSteel)

	IT 131/132	IT 133/134				
Heat Number:	3M74155	3M73212	4M73828	4M73833	4M73835	4M73836
Element	**Wt. %**					
Carbon, C	0.38%	0.38%	0.38%	0.38%	0.38%	0.37%
Manganese, Mn	1.40%	1.34%	1.38%	1.36%	1.38%	1.36%
Silicon, Si	0.56%	0.56%	0.56%	0.54%	0.56%	0.54%
Chromium, Cr	0.16%	0.14%	0.13%	0.15%	0.14%	0.15%
Nickel, Ni	0.08%	0.10%	0.09%	0.10%	0.08%	0.08%
Molybdenum, Mo	0.02%	0.03%	0.03%	0.02%	0.02%	0.02%
Copper, Cu	0.14%	0.17%	0.18%	0.16%	0.18%	0.17%
Phosphorus, P	0.015%	0.010%	0.013%	0.009%	0.013%	0.009%
Sulfur, S	0.058%	0.060%	0.056%	0.054%	0.053%	0.060%
Aluminum, Al	0.004%	0.005%	0.004%	0.003%	0.004%	0.003%
Tin, Sn	0.008%	0.012%	0.010%	0.009%	0.009%	0.008%
Vanadium, V	0.092%	0.086%	0.086%	0.086%	0.082%	0.083%
Columbium, Cb	0.002%	0.002%	0.002%	0.002%	0.002%	0.002%
Boron, B	0.0001%	0.0002%	0.0002%	0.0002%	0.0002%	0.0001%
Calcium, Ca	0.0008%	0.0007%	0.0006%	0.0006%	0.0006%	0.0006%
Titanium, Ti	0.001%	0.001%	0.001%	0.001%	0.001%	0.001%
Nitrogen, N2	0.0148%	0.0159%	0.0150%	0.0147%	0.0151%	0.0151%

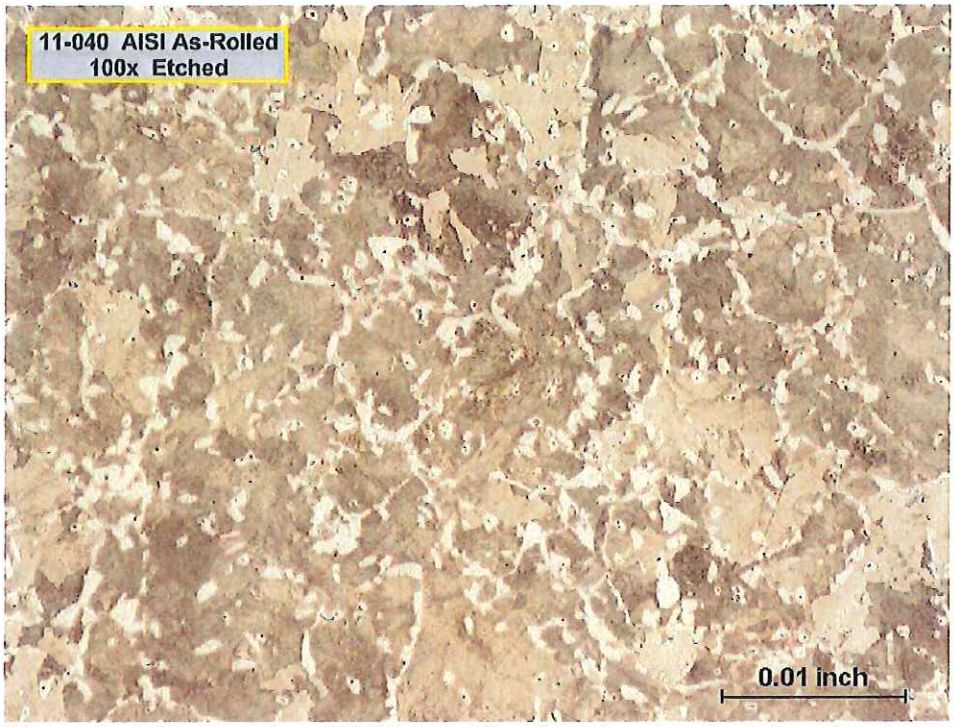

Figure 1: Micrograph at 100X magnification showing the microstructure of 1538MV As-hot Rolled Steel. (Courtesy of Gerdau MacSteel)

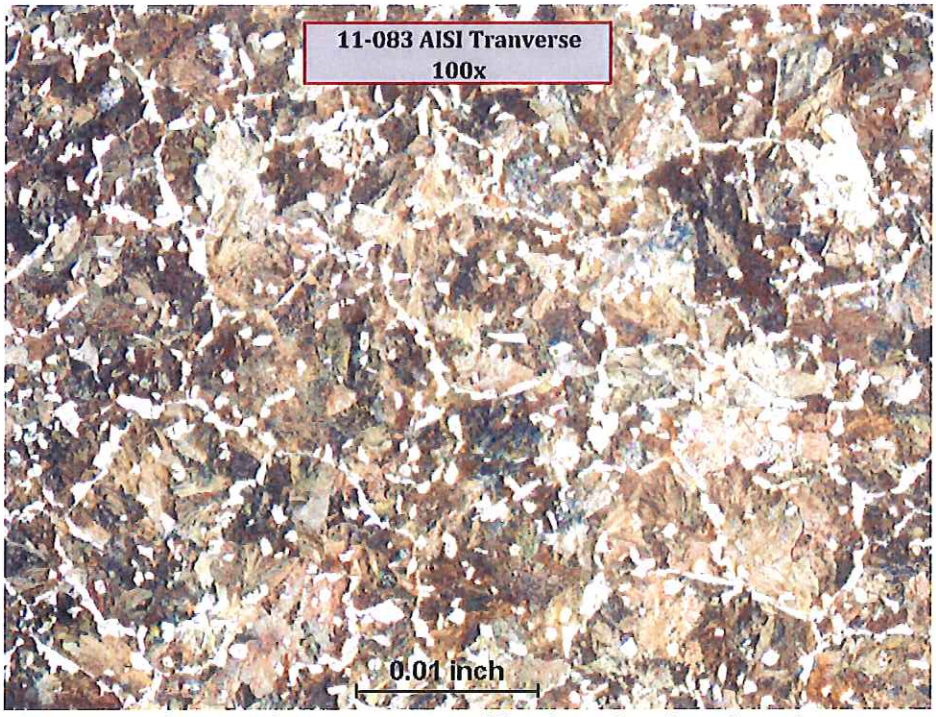

Figure 2: Micrograph at 100X magnification showing the microstructure of 1538MV Forged Steel. (Courtesy of Gerdau MacSteel)

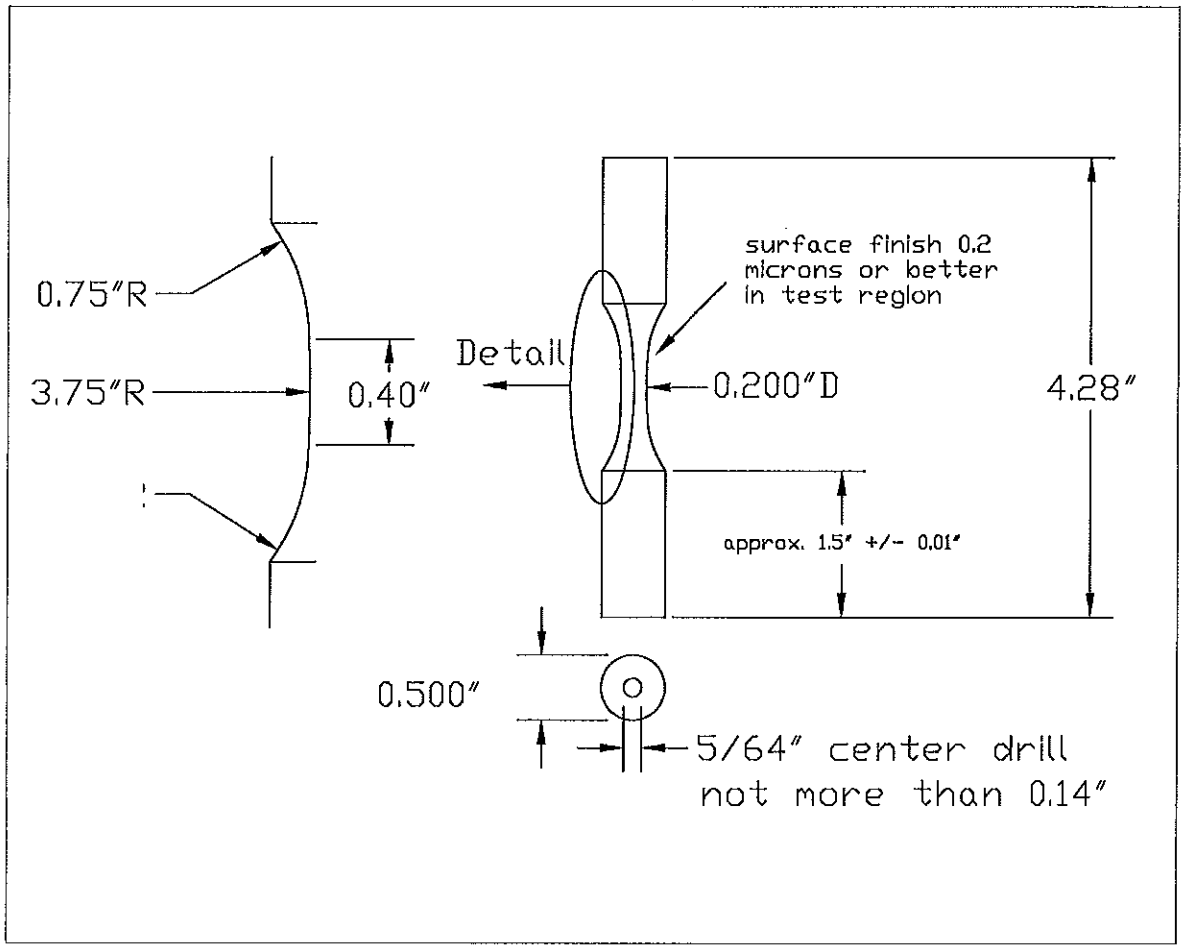

Figure 3: Specimen configuration and dimensions (in.)

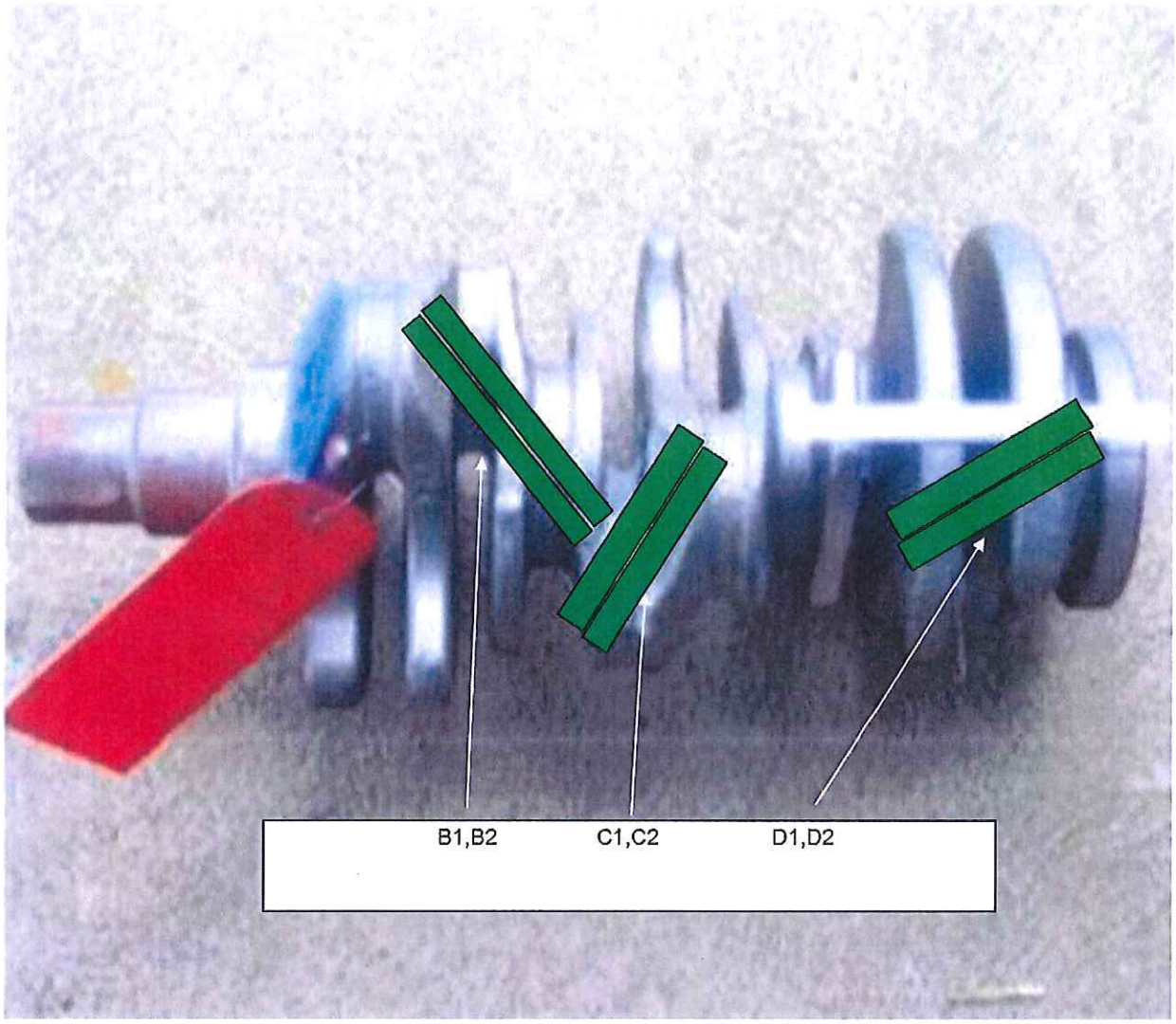

Figure 4: Sections of forged crankshaft used to obtain specimens of iterations 133 and 134

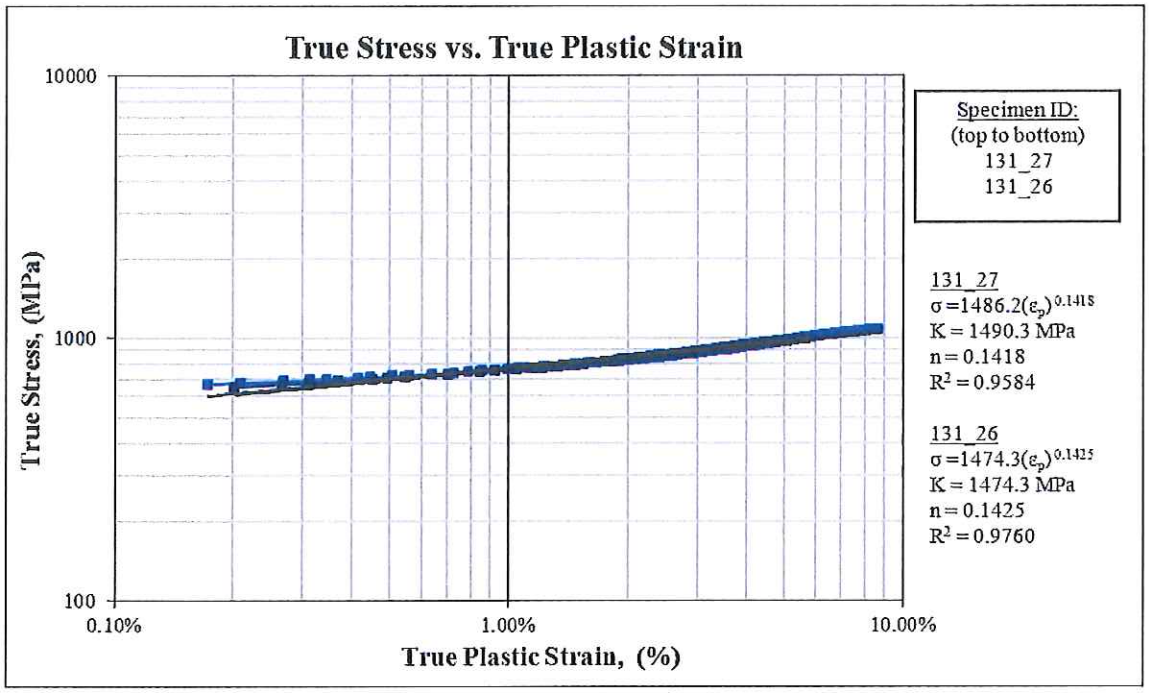

(a)

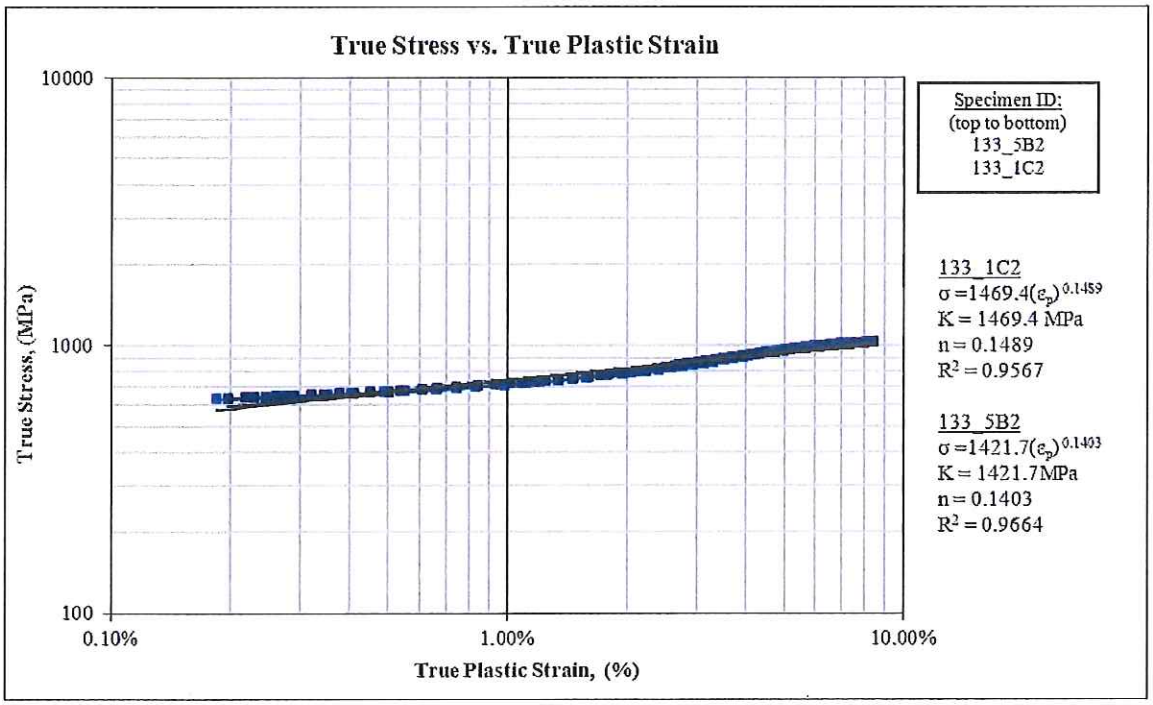

(b)

Figure 5: True stress amplitude versus true plastic strain amplitude (calculated) for (a) IT 131, and (b) IT 133

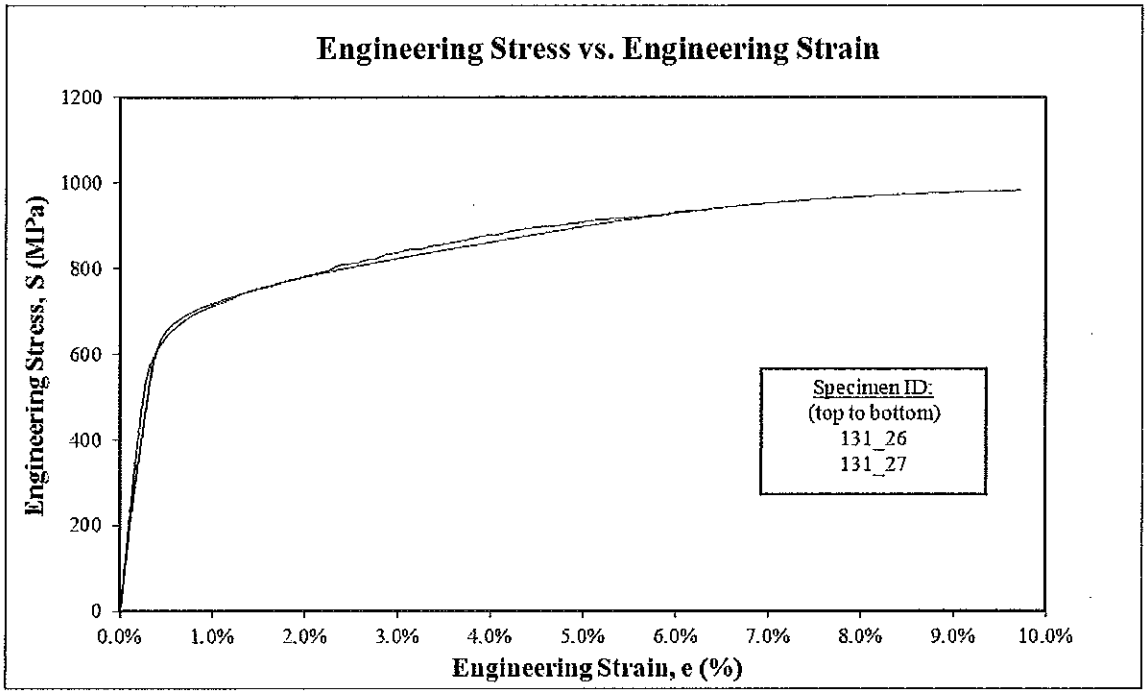

(a)

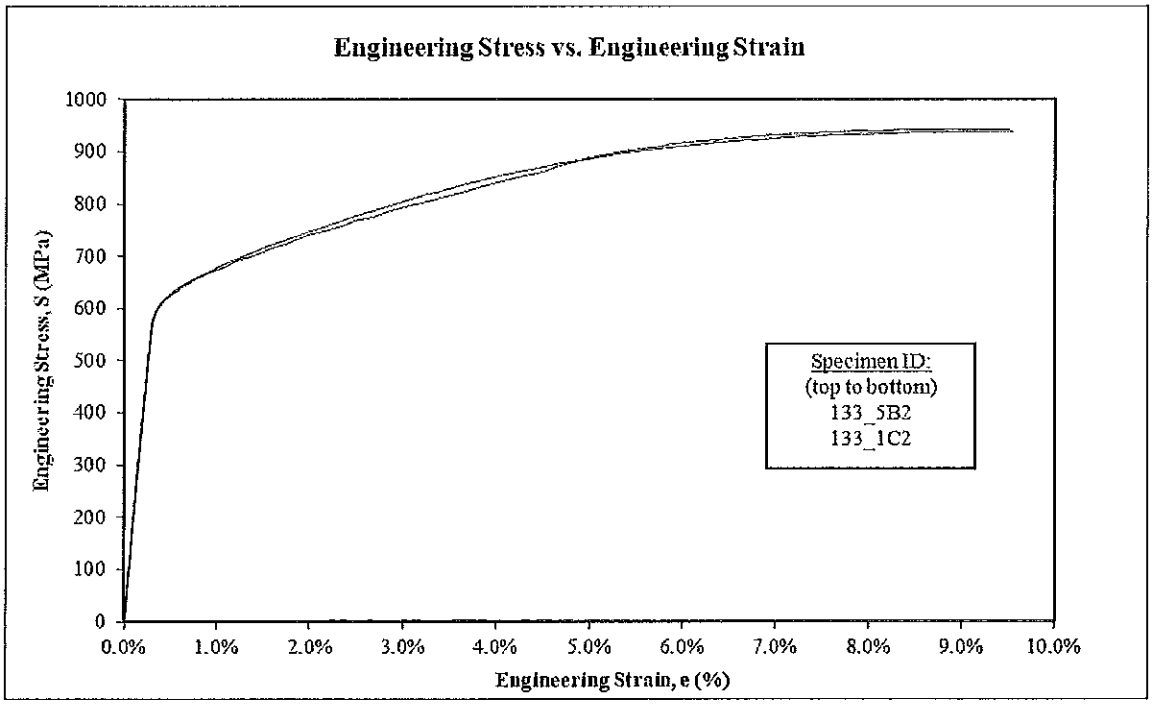

(b)

Figure 6: Monotonic stress-strain curves for (a) IT 131, and (b) IT 133

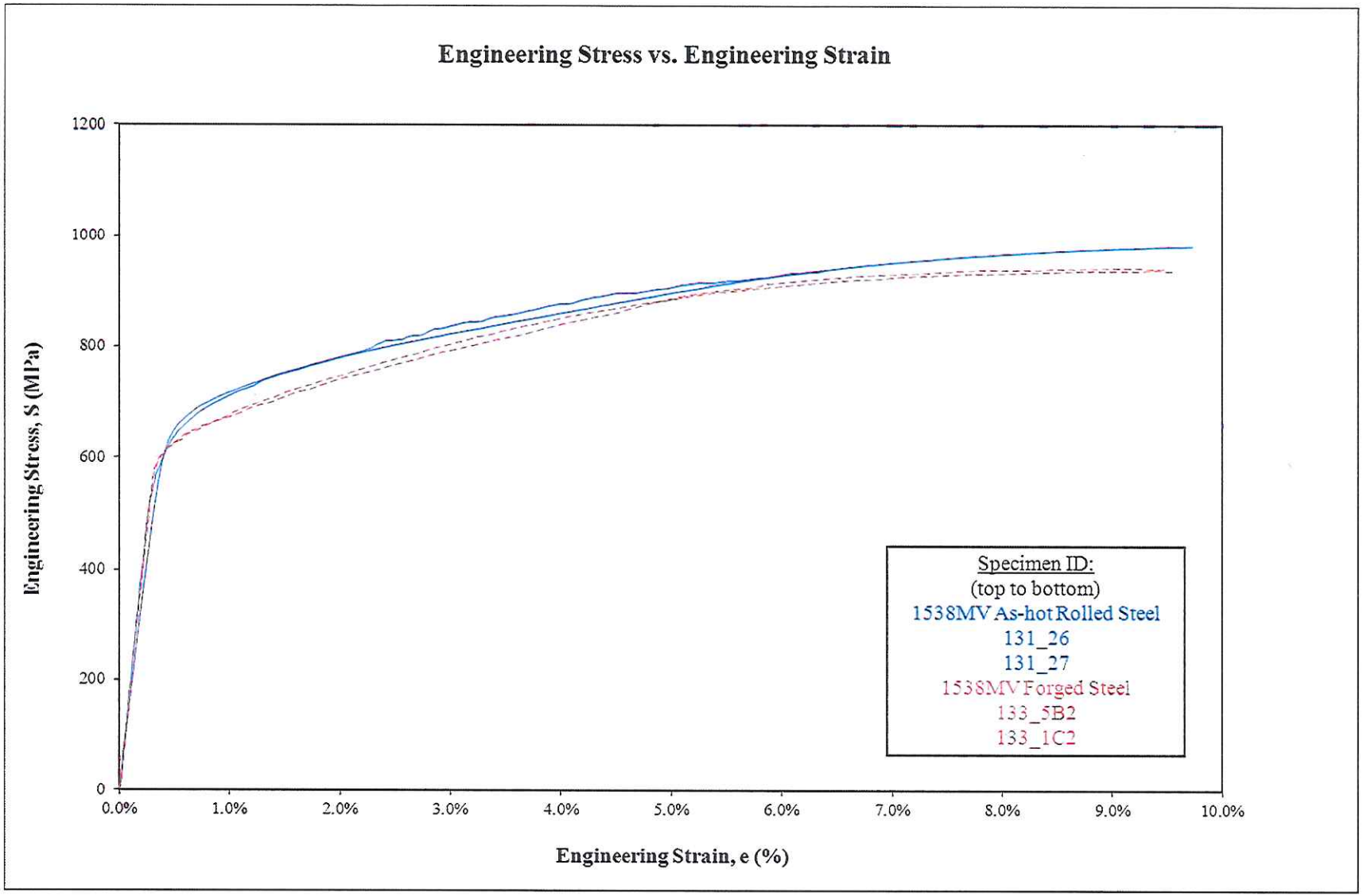

Figure 7: Superimposed monotonic stress-strain curves for IT 131 and 133

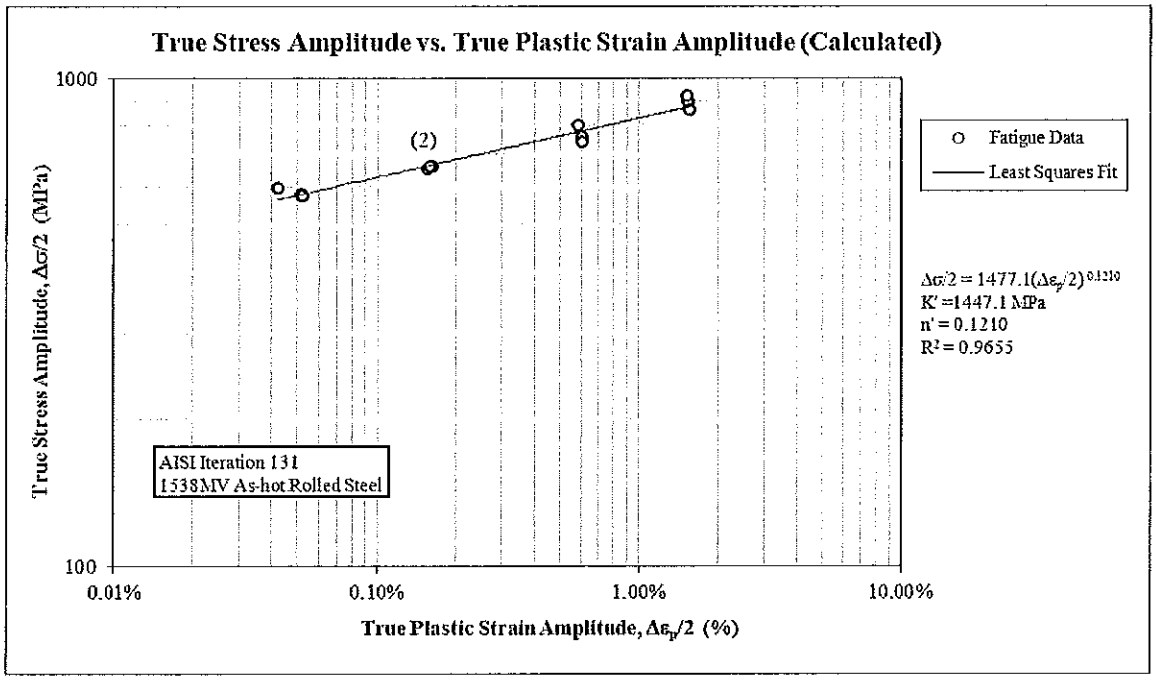

(a)

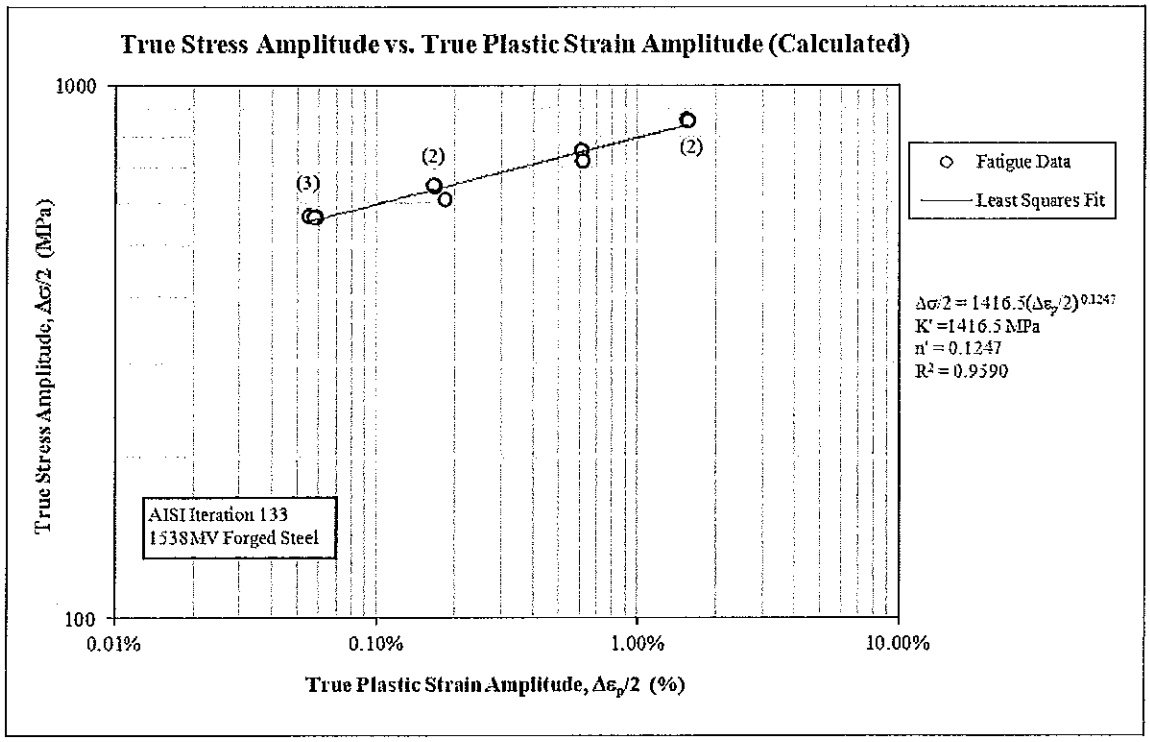

(b)

Figure 8: True stress amplitude versus true plastic strain amplitude (calculated) for (a) IT 131 and (b) IT 133

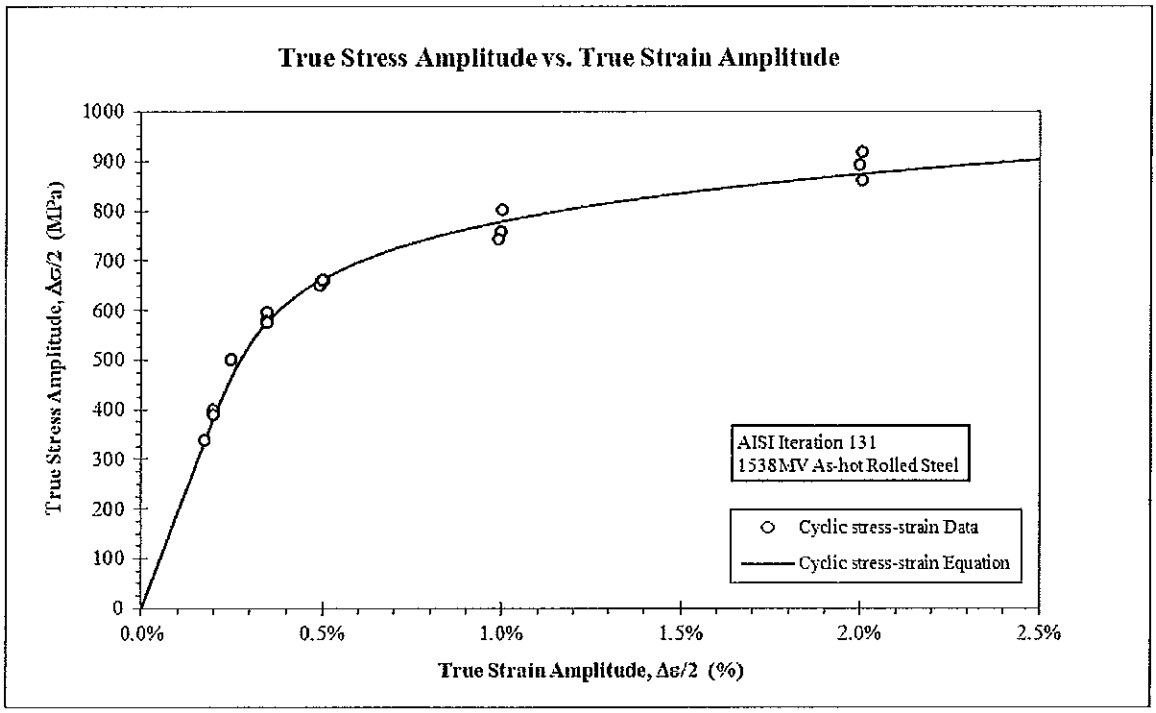

(a)

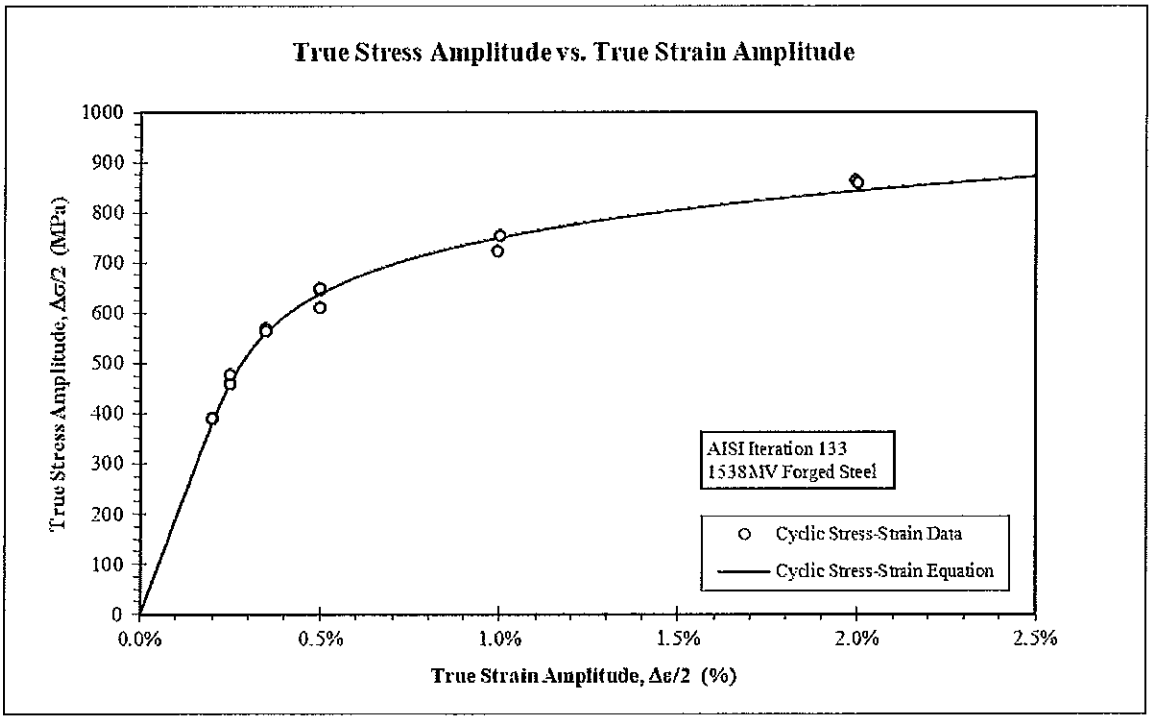

(b)

Figure 9: True stress amplitude versus true strain amplitude for (a) IT 131 and (b) IT 133

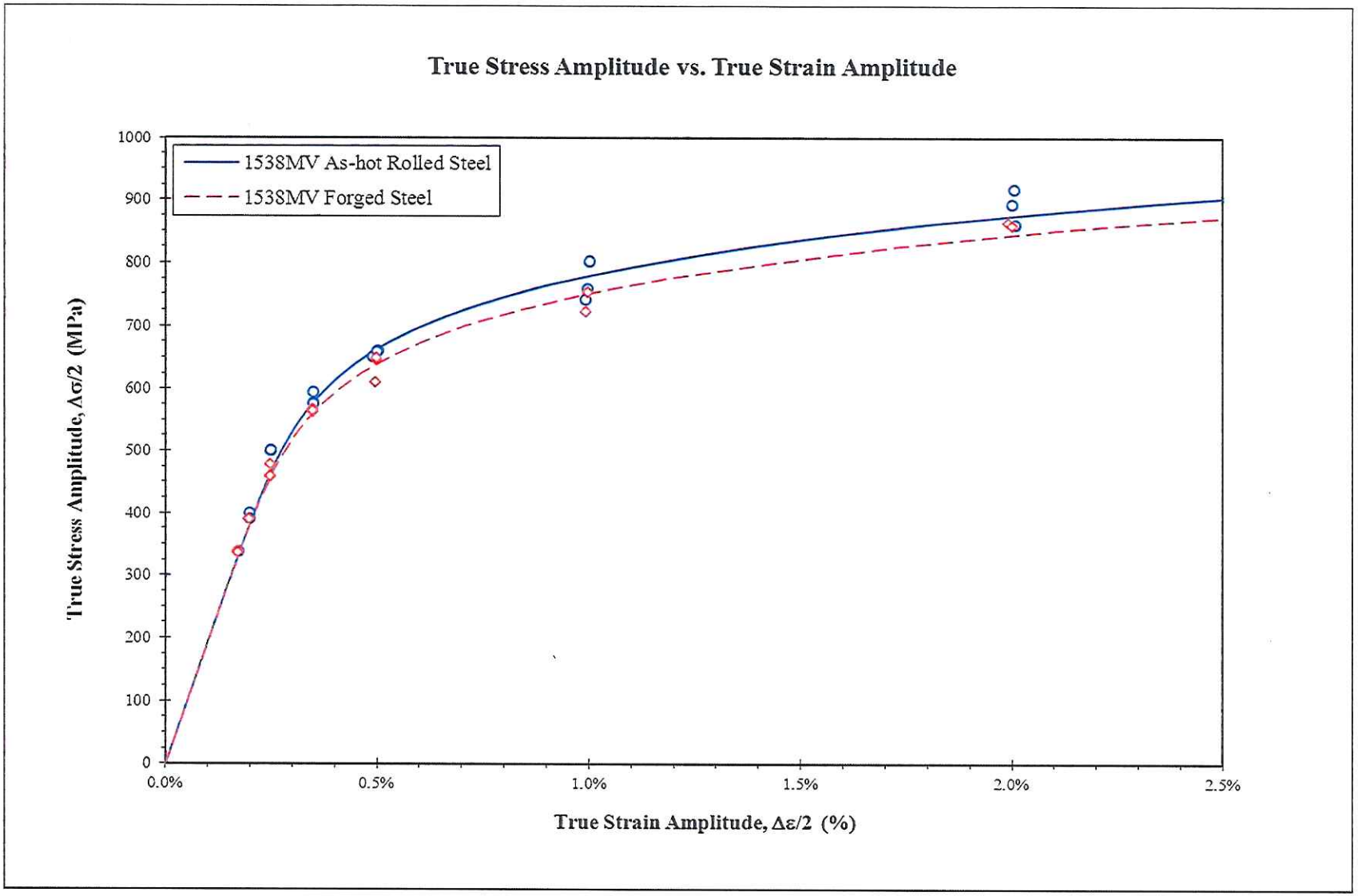

Figure 10: Superimposed true stress amplitude versus true strain amplitude data for IT 131 and 133

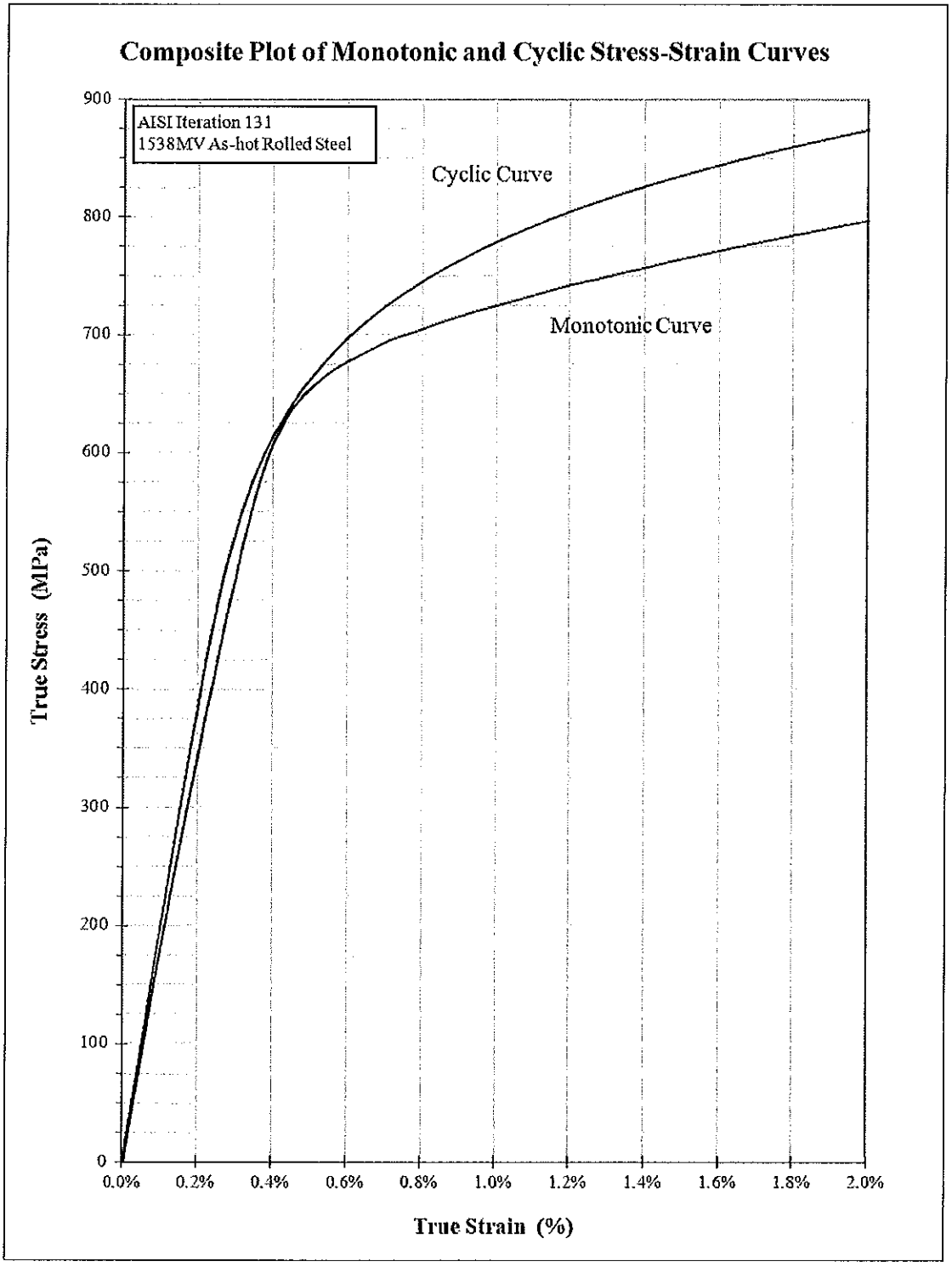

Figure 11: Composite plot of cyclic and monotonic stress-strain curves for IT 131

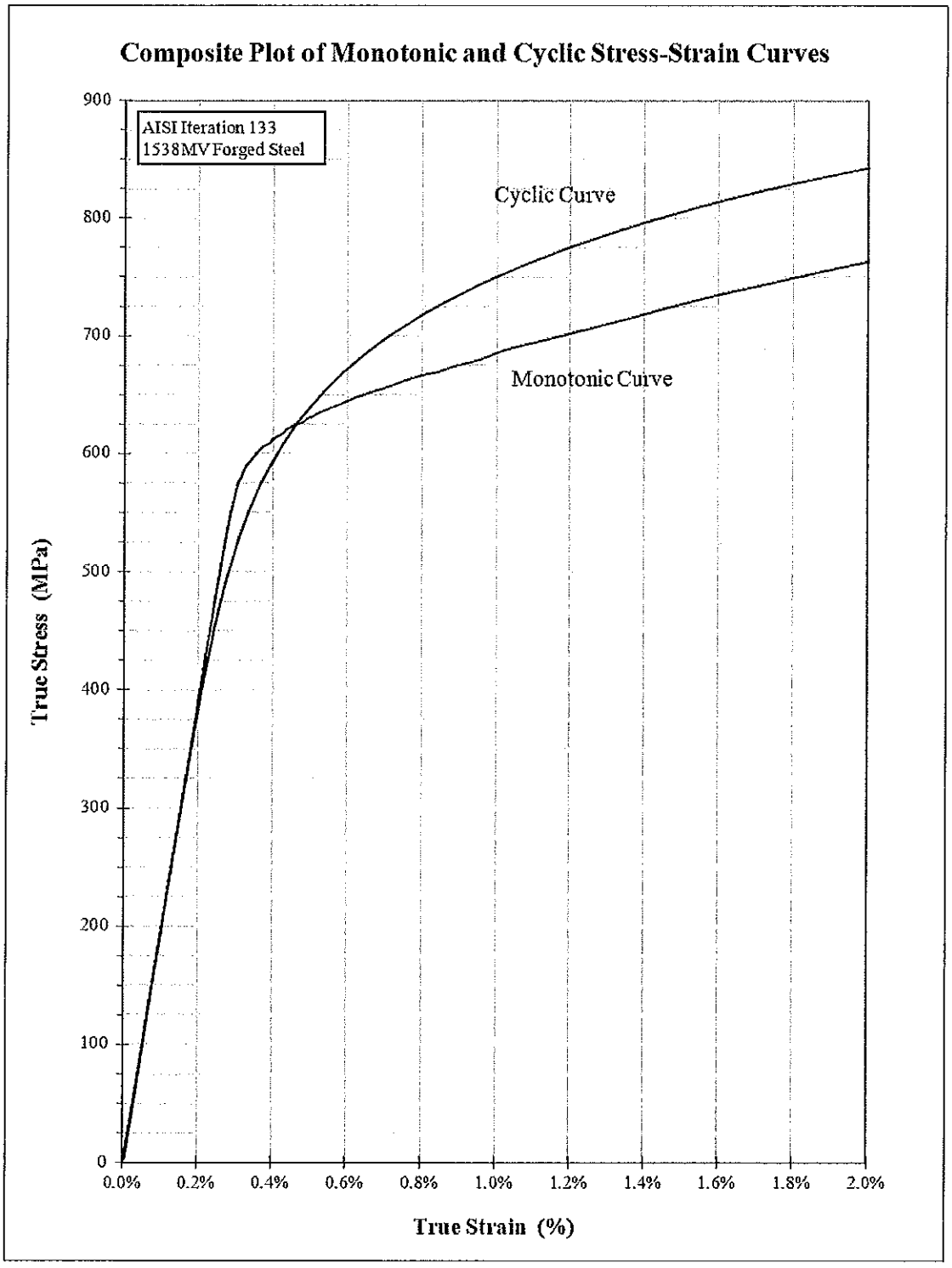

Figure 12: Composite plot of cyclic and monotonic stress-strain curves for IT 133

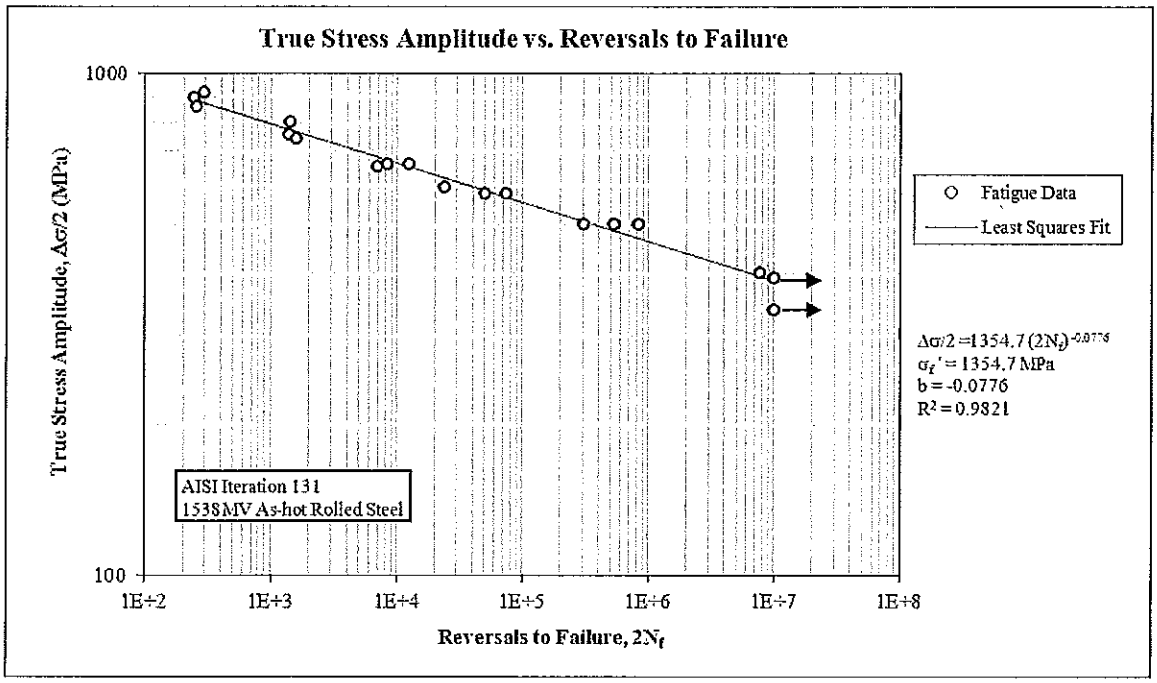

(a)

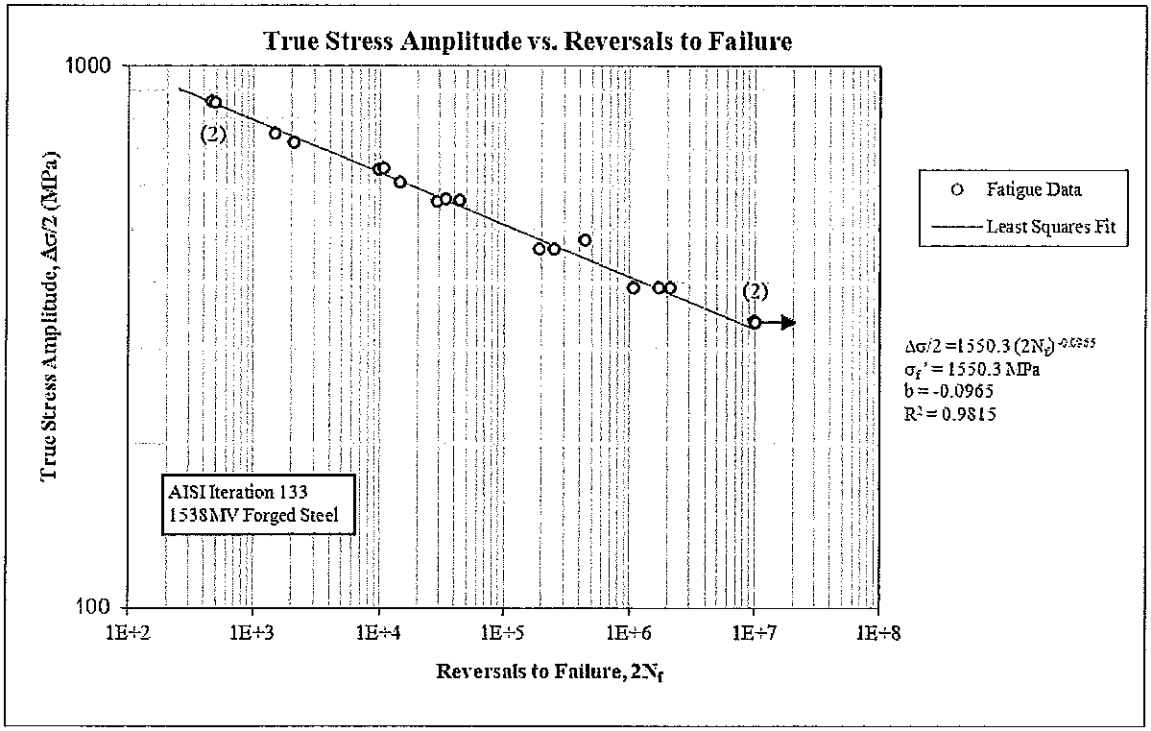

(b)

Figure 13: True stress amplitude versus reversals to failure for (a) IT 131 and (b) IT 133

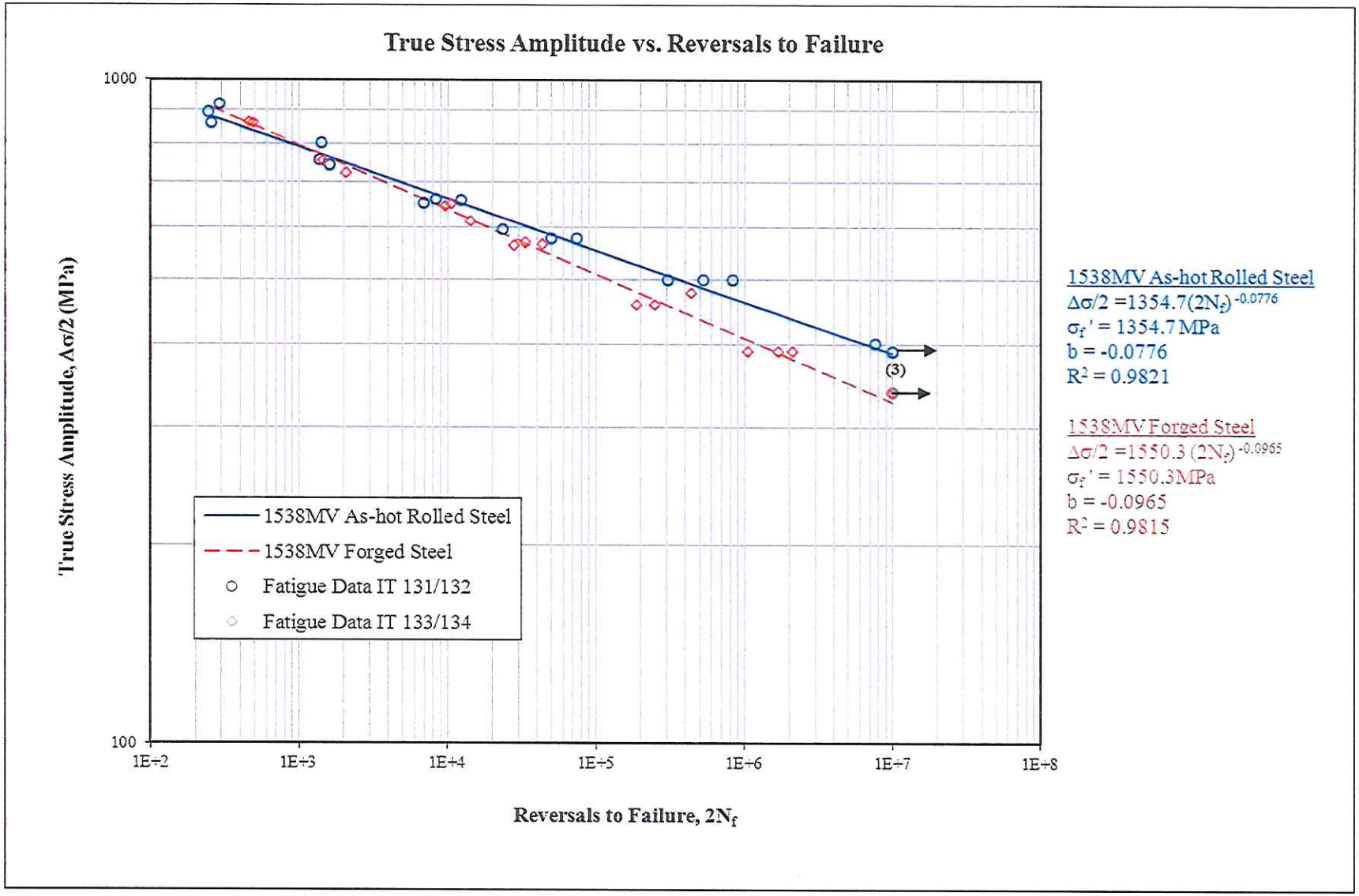

Figure 14: Superimposed true stress amplitude versus reversals to failure data for IT 131 and 133

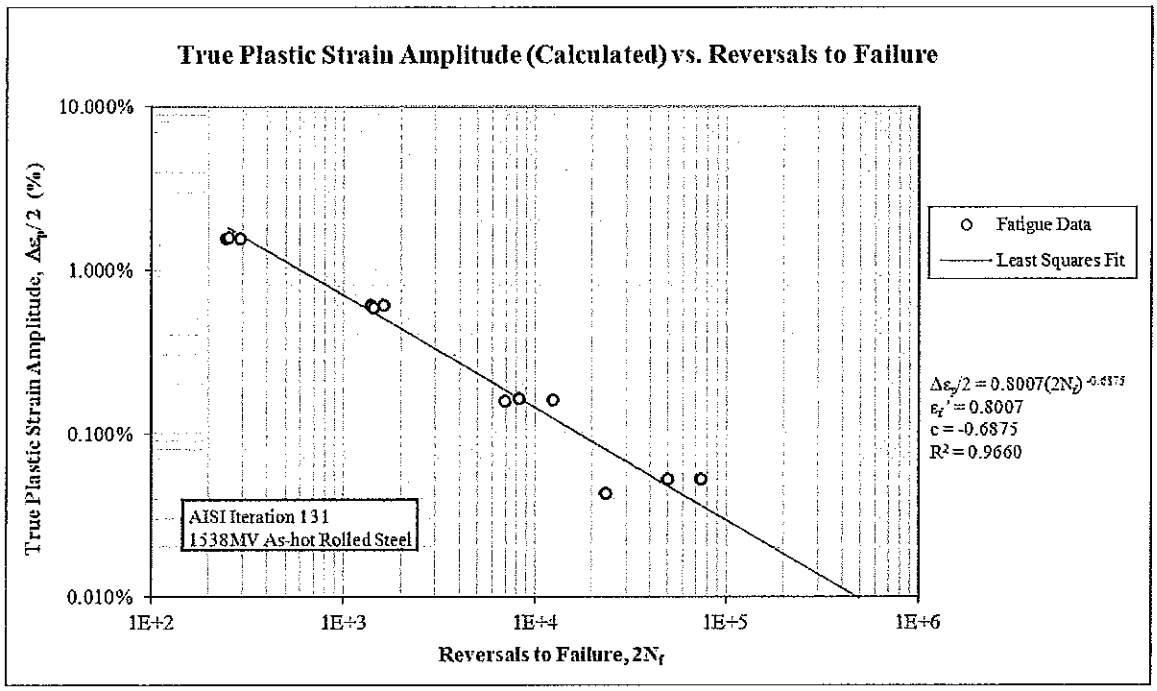

(a)

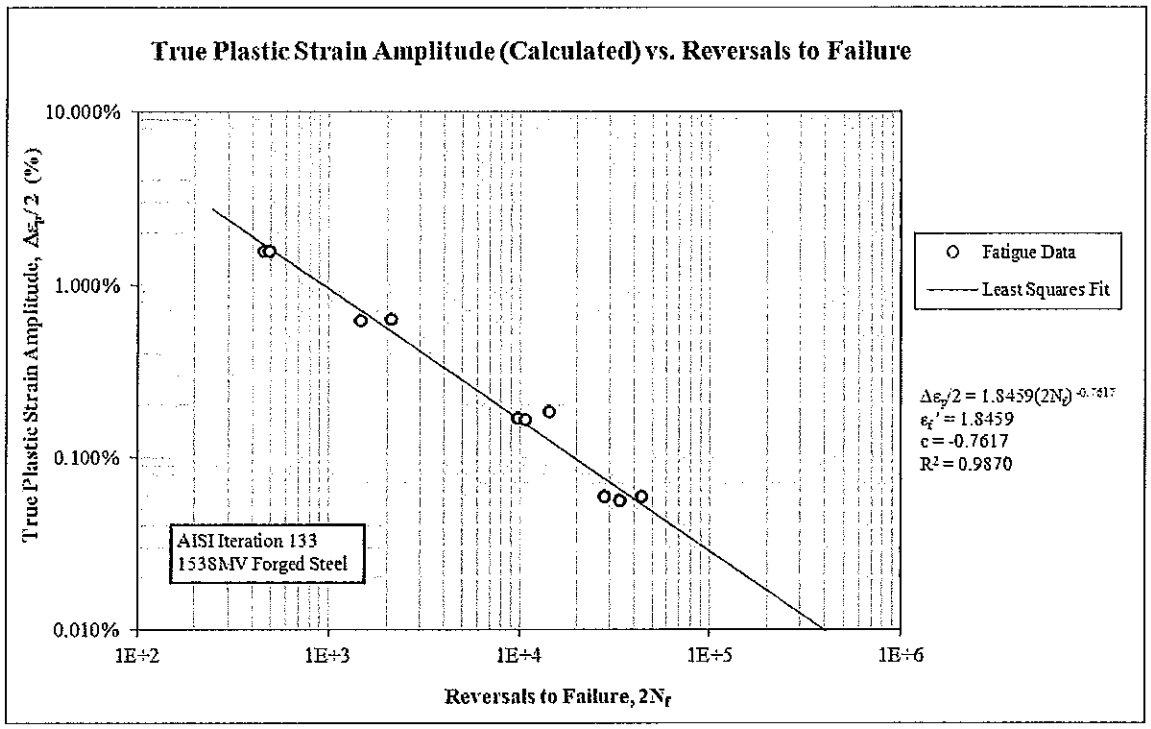

(b)

Figure 15: True plastic strain amplitude (calculated) versus reversals to failure for (a) IT 131 and (b) and IT 133

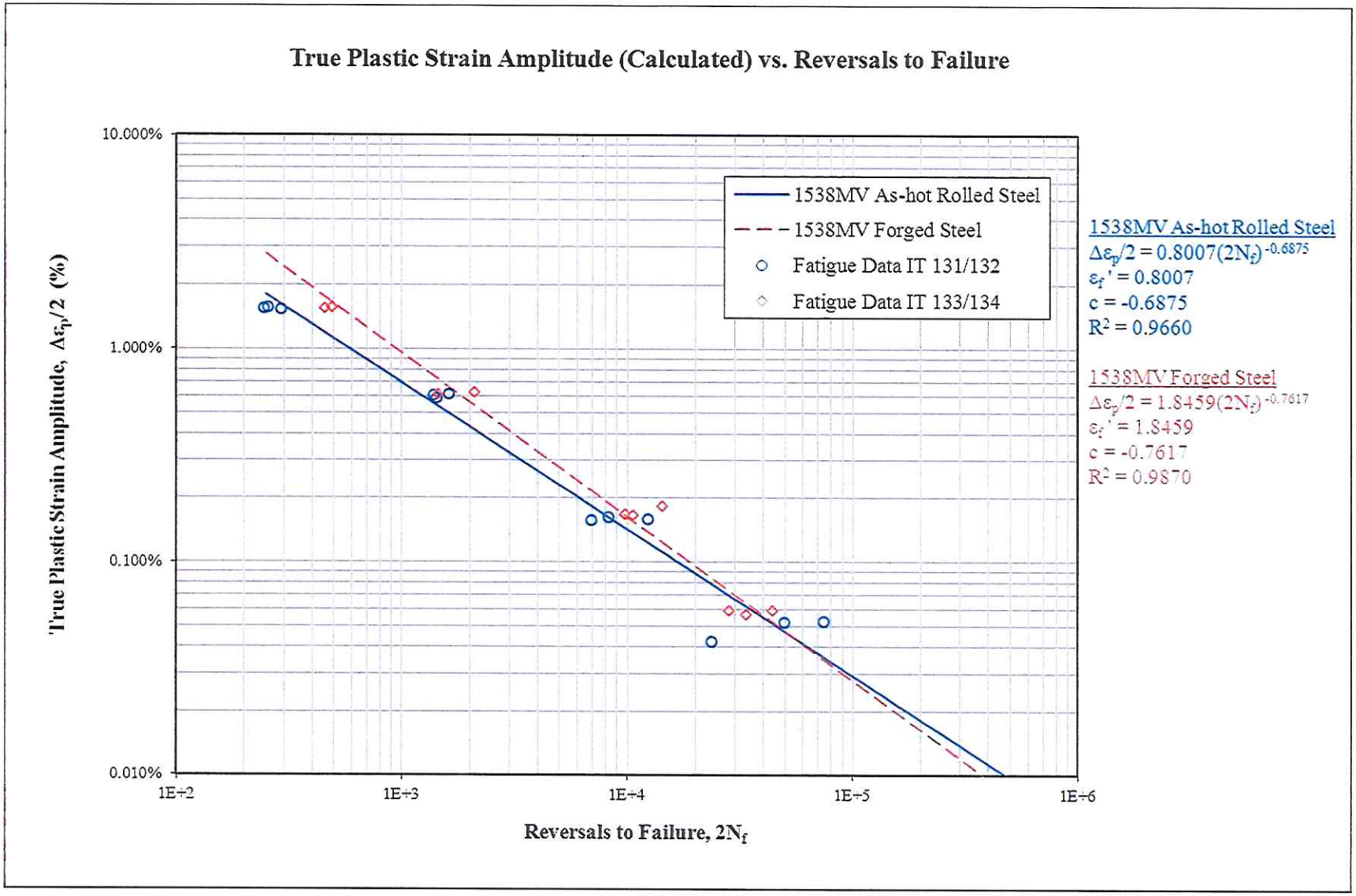

Figure 16: Superimposed true plastic strain amplitude (calculated) versus reversals to failure data for IT 131 and 133

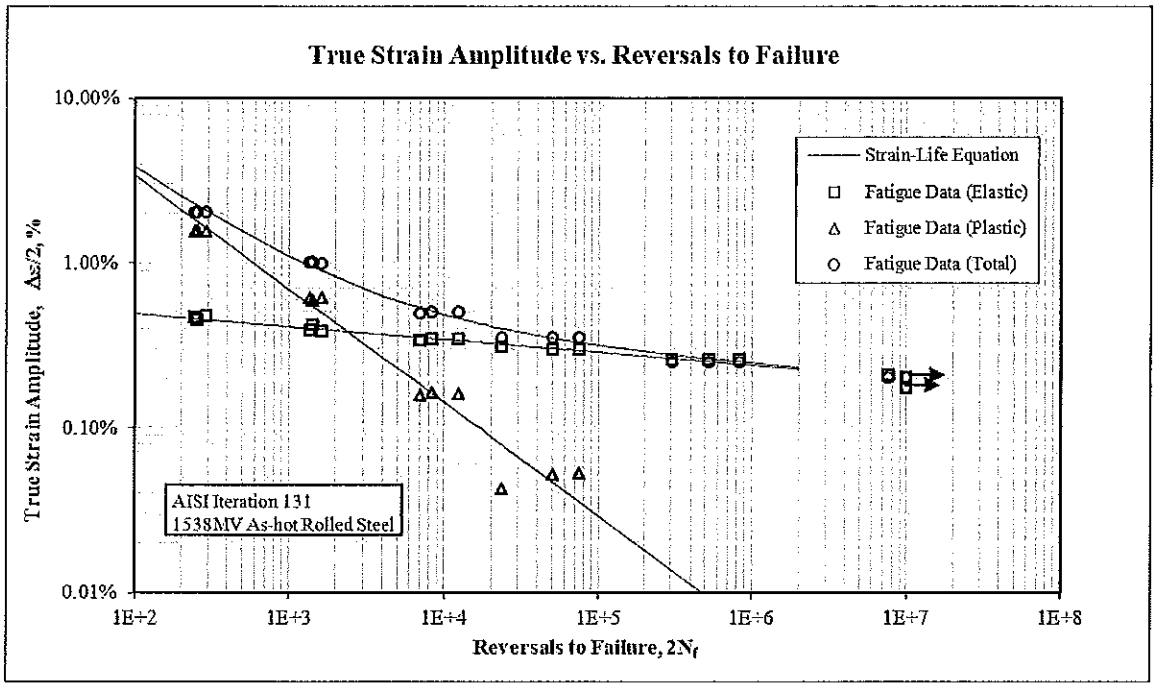

(a)

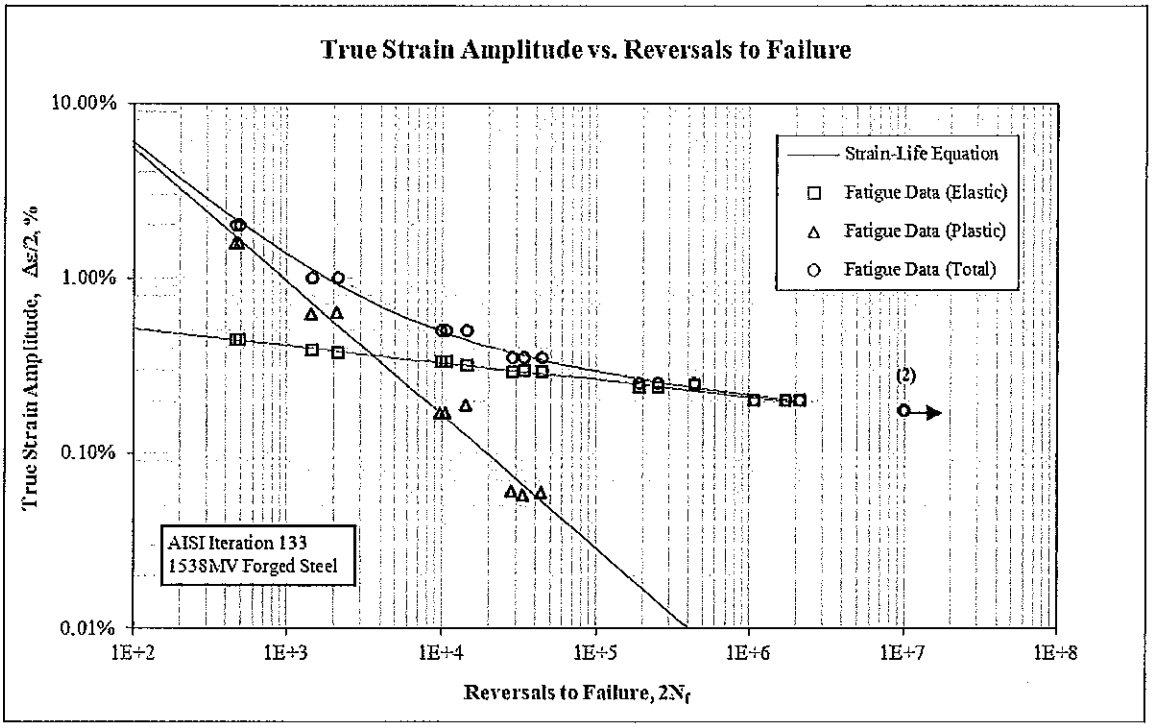

(b)

Figure 17: True strain amplitude versus reversals to failure for (a) IT 131 and (b) IT 133

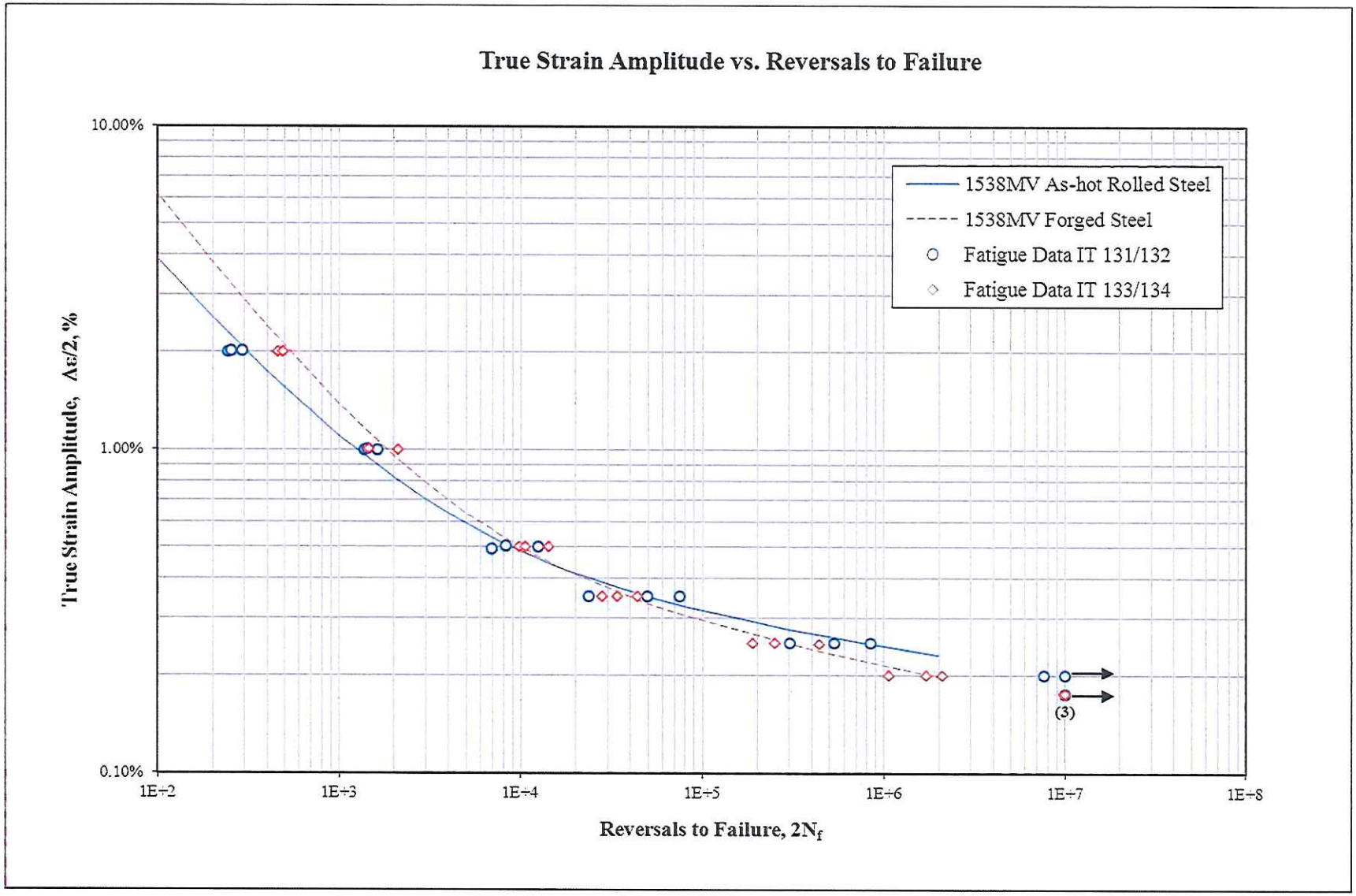

Figure 18: Superimposed true strain amplitude versus reversals to failure data for IT 131 and 133

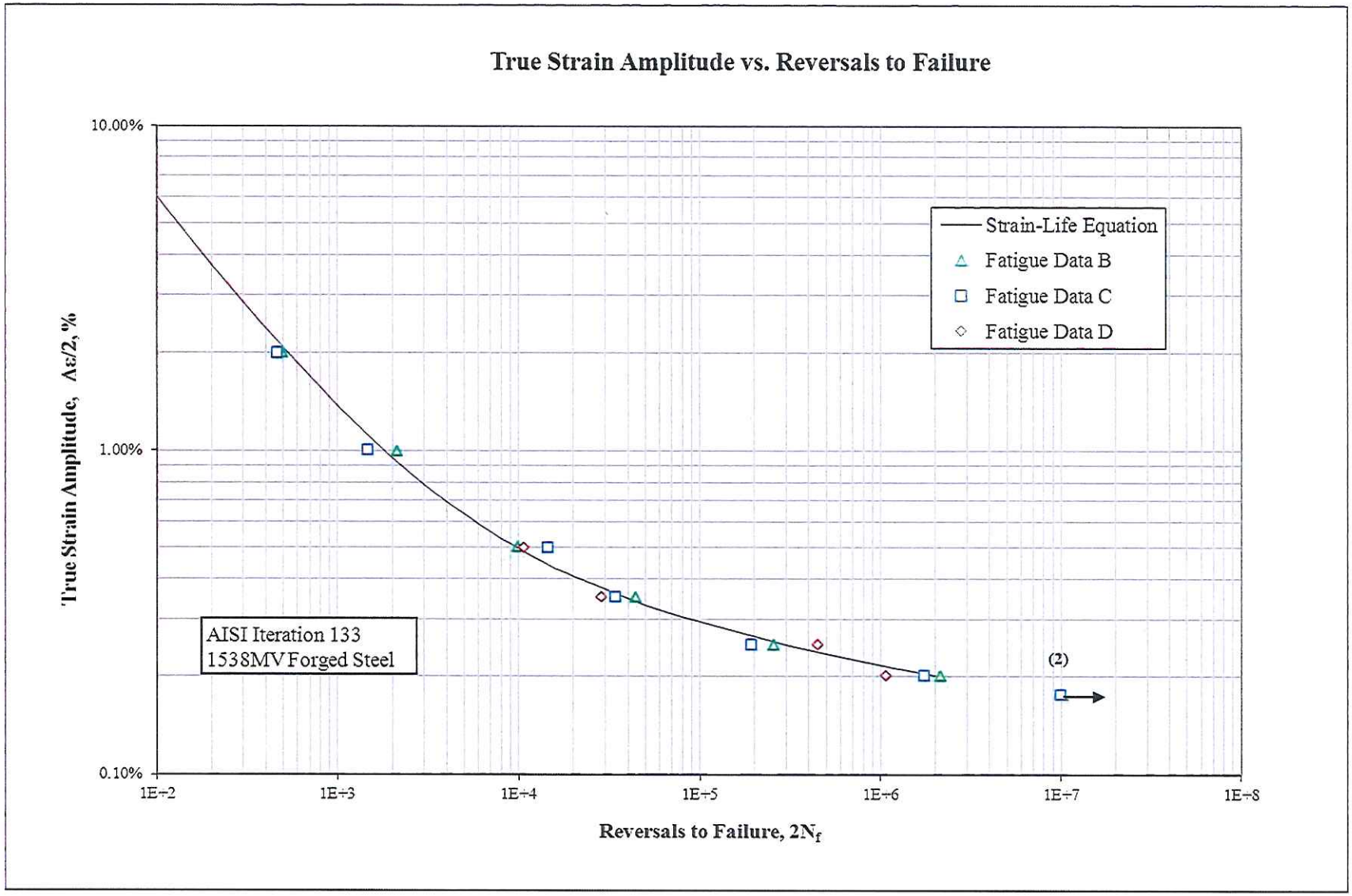

Figure 19: Superimposed true strain amplitude versus reversals to failure data from various crankshaft sections

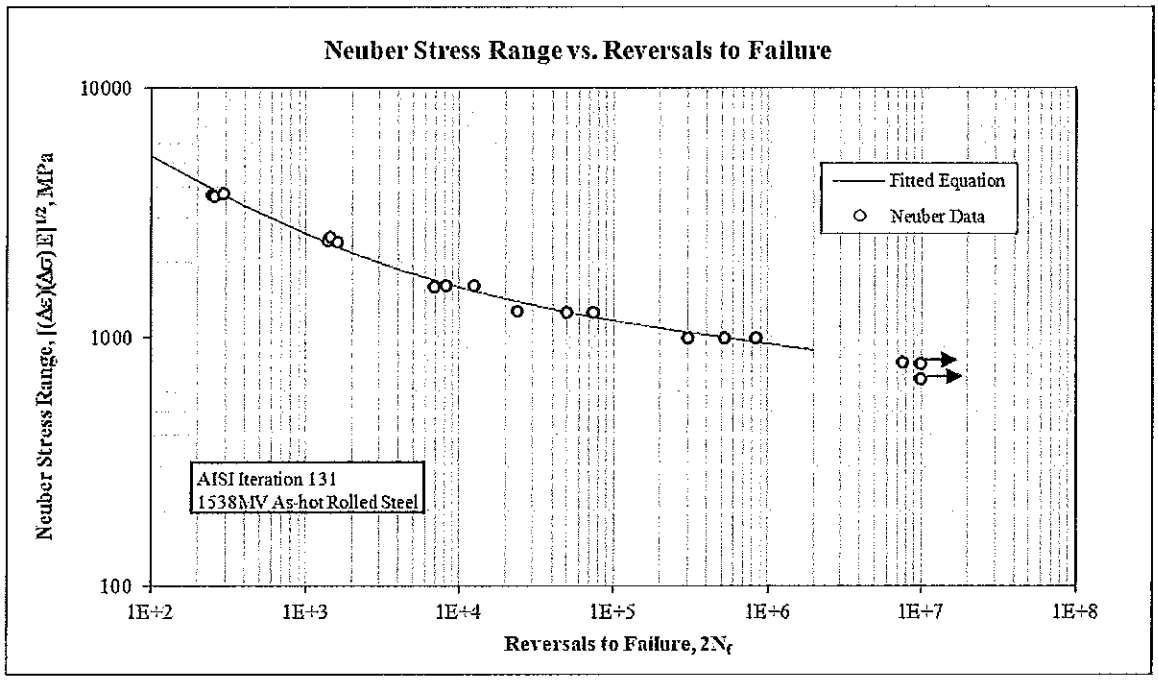

(a)

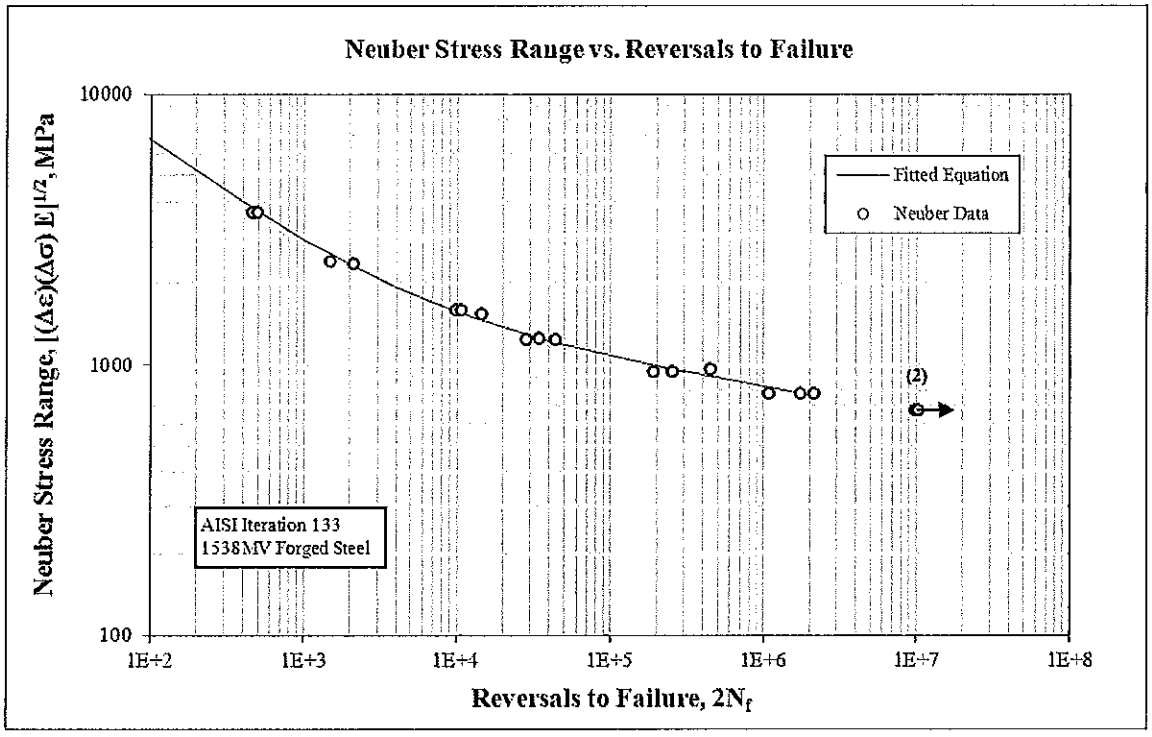

(b)

Figure 20: Neuber stress range versus reversals to failure for (a) IT 131 and (b) IT 133

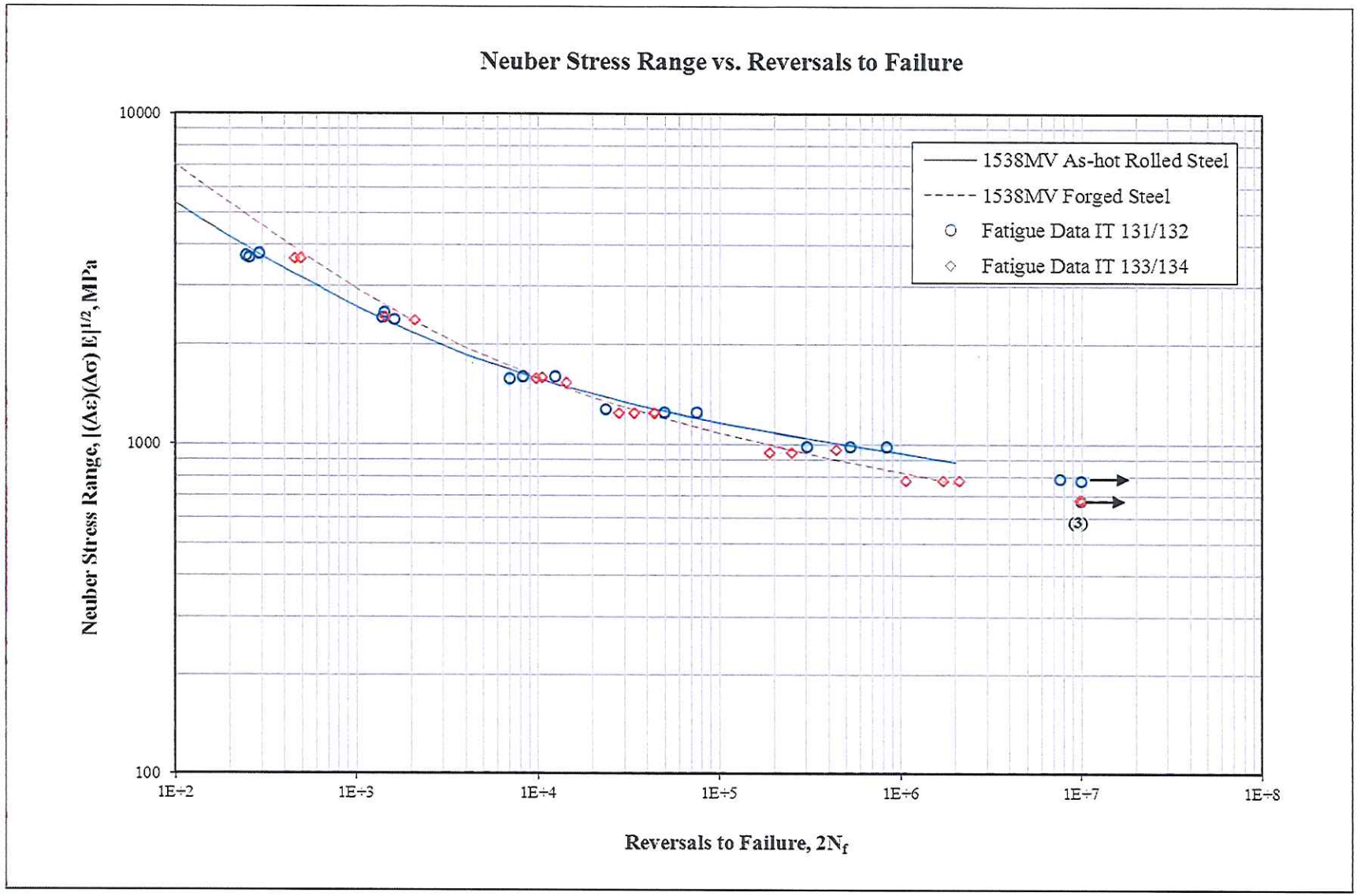

Figure 21: Superimposed neuber stress range versus reversals to failure data for IT 131 and 133

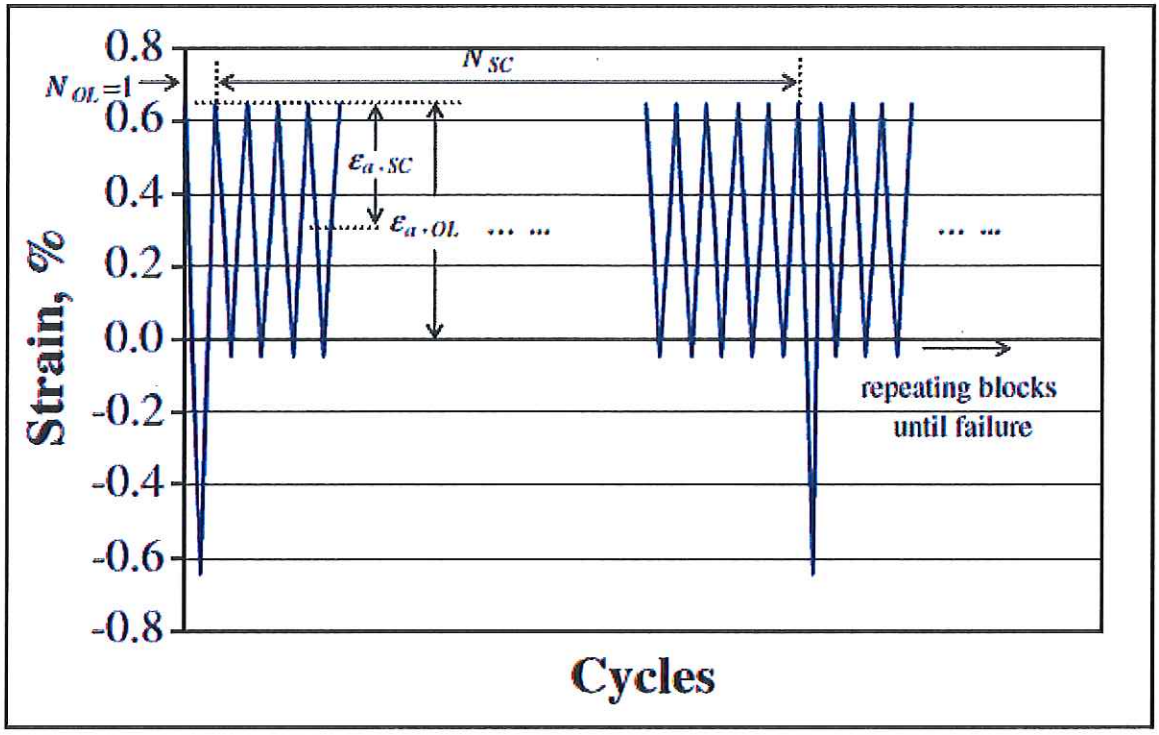

Figure 22: Periodic overload history

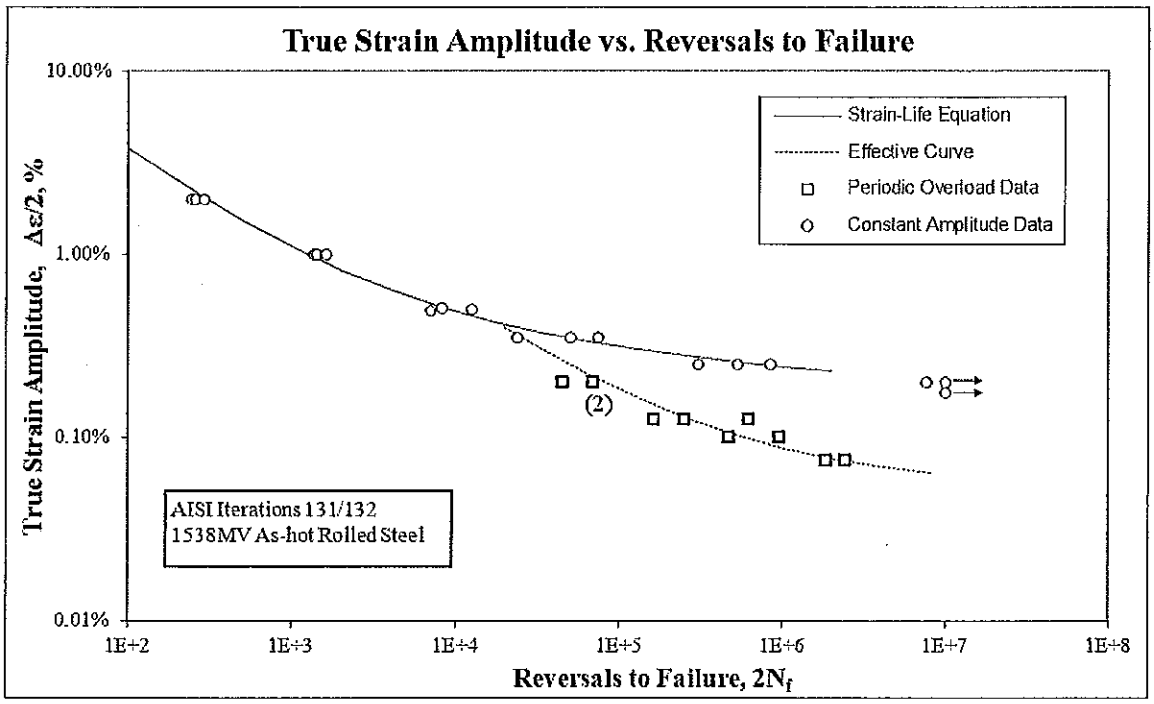

(a)

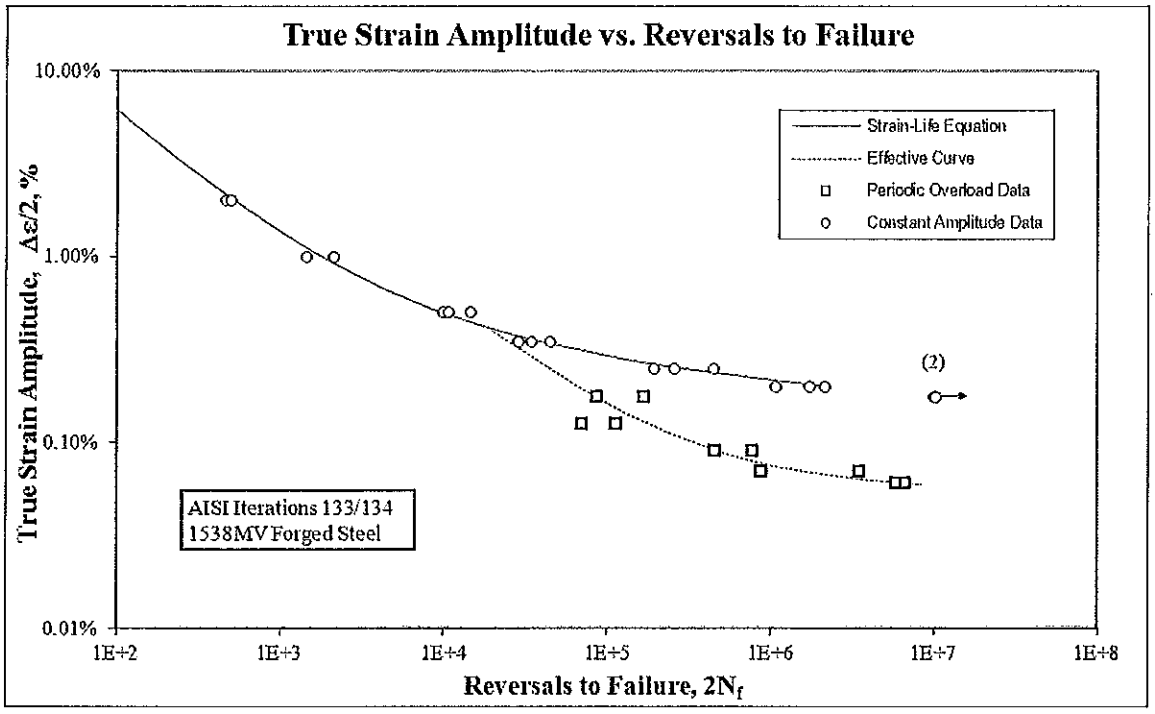

(b)

Figure 23: Periodic overload data superimposed with constant amplitude fatigue data for (a) IT 131/132 and (b) IT 133/134

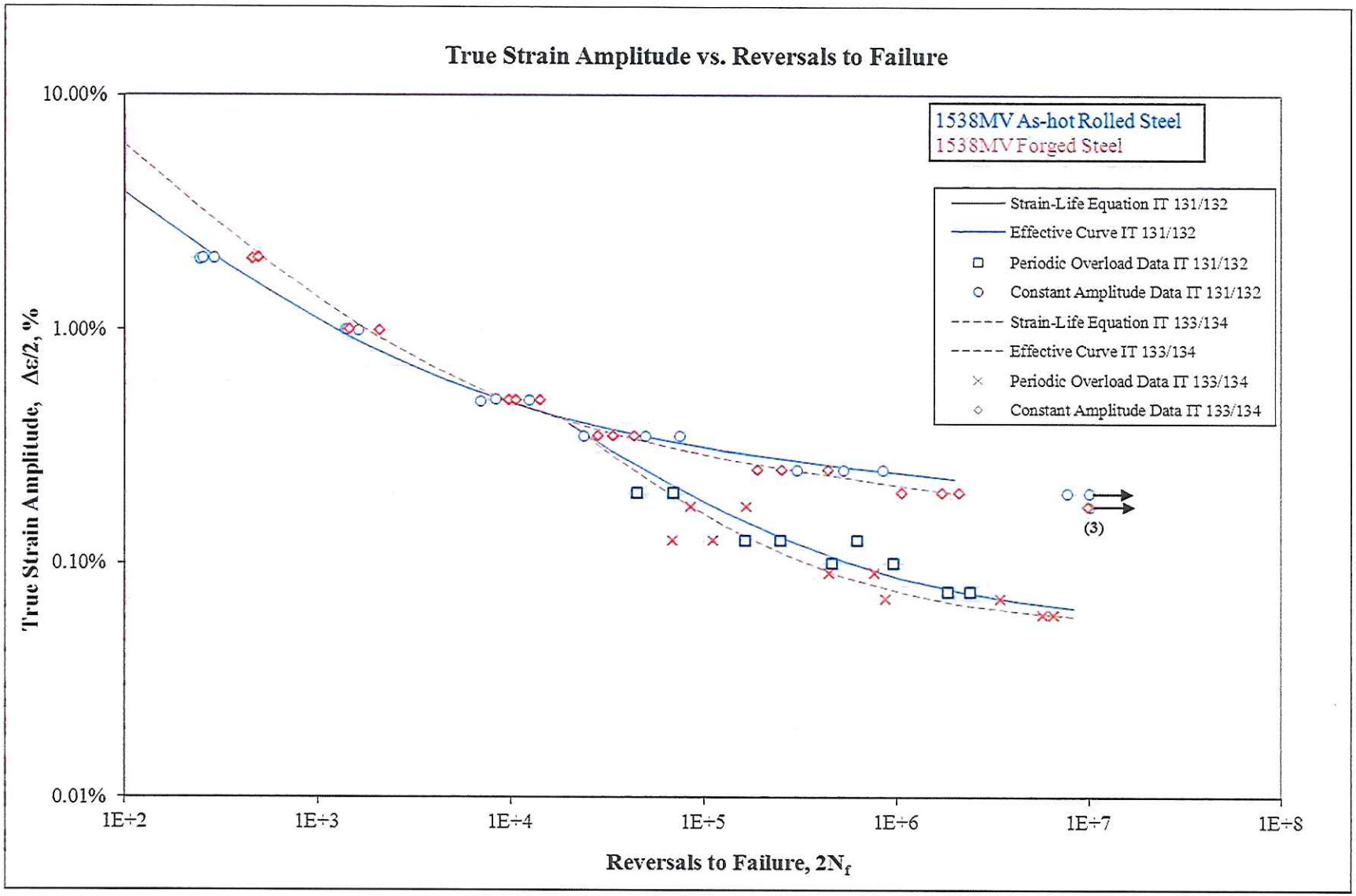

Figure 24: Periodic overload data superimposed with constant amplitude fatigue data for IT 131/132 and 133/134

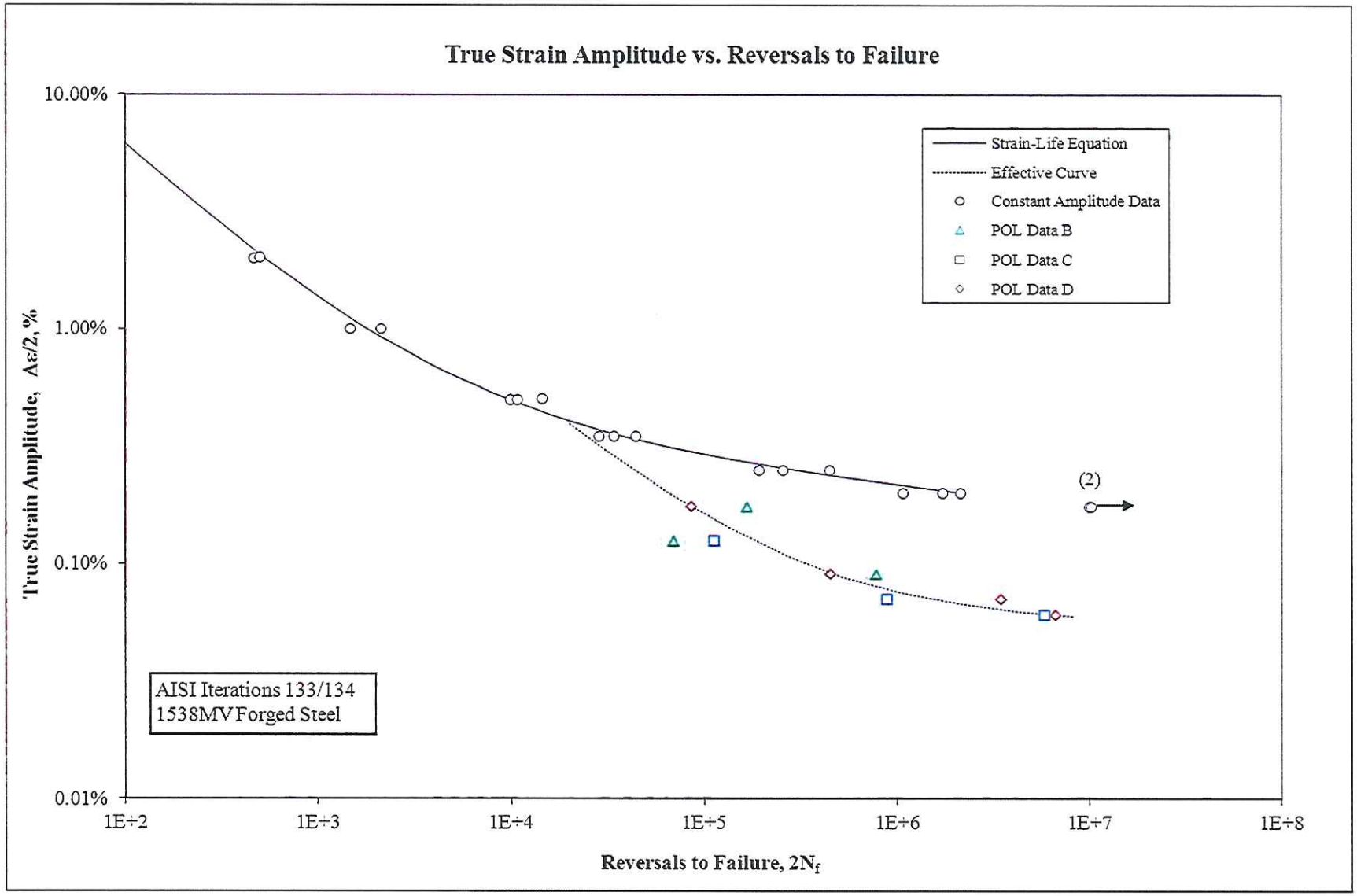

Figure 25: Periodic overload data from specimens of various crankshaft sections for IT 133/134

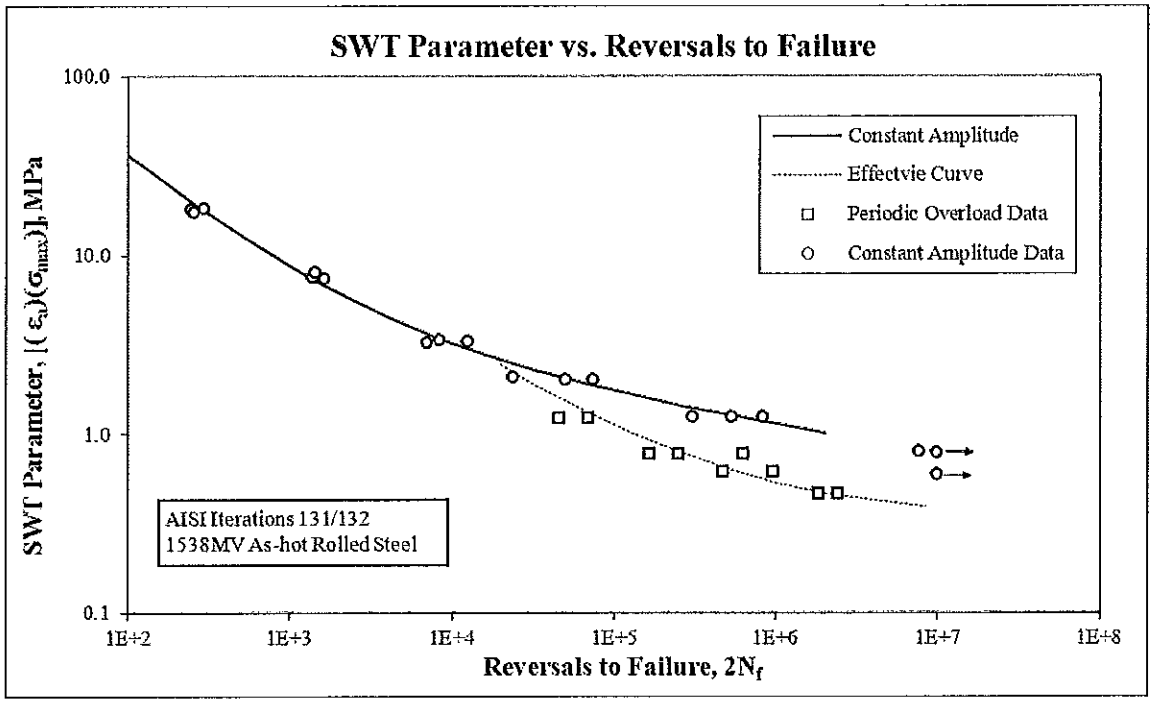

(a)

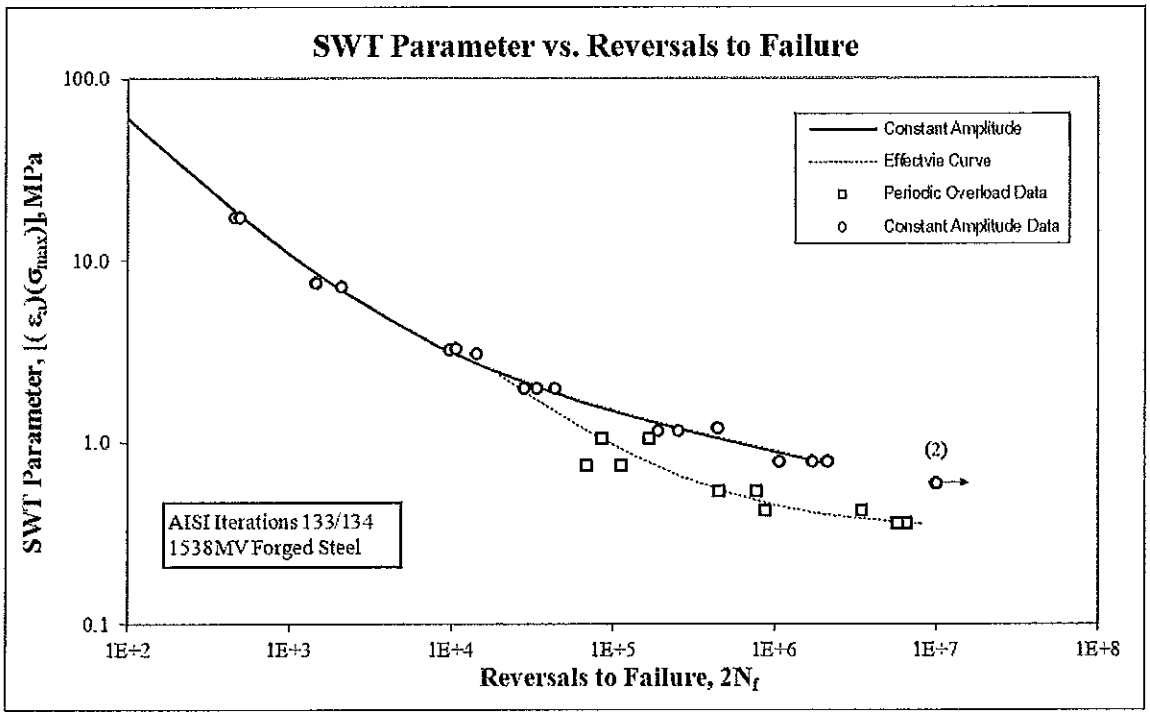

(b)

Figure 26: Periodic overload data superimposed with constant amplitude data in a plot of SWT parameter versus reversals to failure for (a) IT 131/132 and (b) IT 133/134

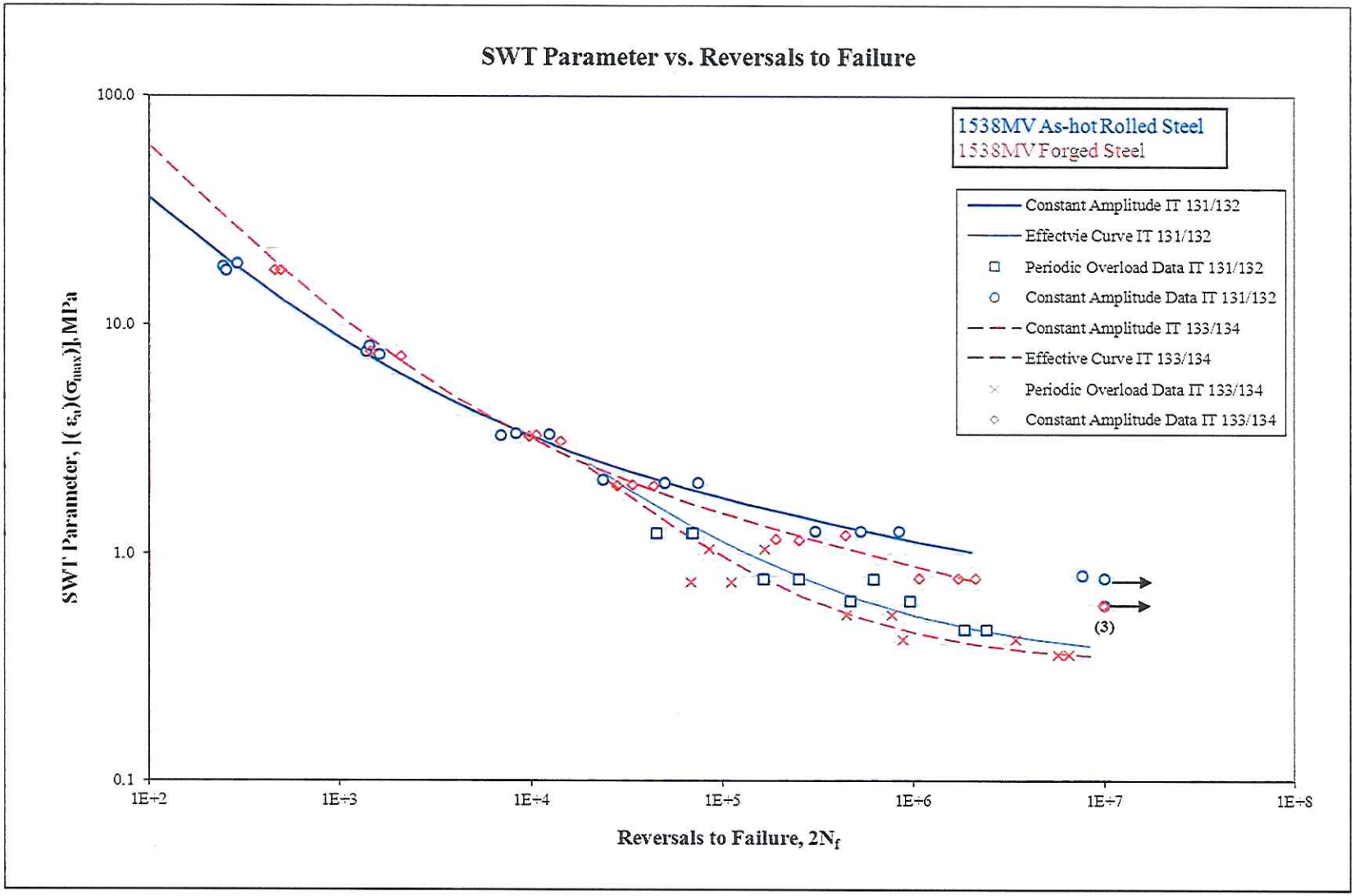

Figure 27: Periodic overload and constant amplitude data in a plot of SWT parameter for IT 131/132 and 133/134

REFERENCES

[1] ASTM Standard E606-92, "Standard Practice for Strain-Controlled Fatigue Testing," Annual Book of ASTM Standards, Vol. 03.01, 2004, pp. 593-606.

[2] ASTM Standard E83-02, "Standard Practice for Verification and Classification of Extensometers," Annual Book of ASTM Standards, Vol. 03.01, 2004, pp. 232-244.

[3] ASTM Standard E1012-99, "Standard Practice for Verification of Specimen Alignment Under Tensile Loading," Annual Book of ASTM Standards, Vol. 03.01, 2004, pp. 763-770.

[4] ASTM Standard E8-04, "Standard Test Methods for Tension Testing of Metallic Materials," Annual Book of ASTM Standards, Vol. 03.01, 2004, pp. 62-85.

[5] ASTM Standard E739-91, "Standard Practice for Statistical Analysis of Linear or Linearized Stress-Life (S-N) and Strain-Life (ε-N) Fatigue Data," Annual Book of ASTM Standards, Vol. 03.01, 1995, pp. 670-676.

[6] ASTM Standard E646-00, "Standard Test Method for Tensile Strain-Hardening Exponents (n-values) of Metallic Sheet Materials," Annual Book of ASTM Standards, Vol. 03.01, 2004, pp. 619-626.

[7] Stephens R. I., Fatemi A., Stephens R. R. and Fuchs H. O., "*Metal Fatigue in Engineering*", Second edition, Wiley Interscience, 2000.

APPENDIX A

Table A-1: Summary of monotonic tensile test results from IT 131 and 133

Specimen ID	D_o, mm (in)	D_f, mm (in)	L_o, mm (in)	L_f, mm (in)	R, mm (in)	E, Gpa (ksi)	YS (offset=0.2%), Mpa (ksi)	S_u, Mpa (ksi)	K, Mpa (ksi)	n	%EL	%RA	ε_f, %	σ_f, Mpa (ksi)
131_26	5.210 (0.2051)	4.350 (0.1713)	5.850 (0.2303)	7.45 (0.2933)	2.223 (0.0875)	201.5 (29,224)	640.0 (92.8)	958.3 (139.0)	1474.3 (213.8)	0.1425	27.4%	30.3%	36.1%	1029.6 (149.3)
131_27	5.160 (0.2031)	4.430 (0.1744)	6.250 (0.2461)	7.65 (0.3012)	2.540 (0.1000)	184.8 (26,802)	660.5 (95.8)	988.4 (143.4)	1486.2 (215.5)	0.1418	22.4%	26.3%	30.5%	1047.9 (152.0)
Average Values						193.2 (28,013)	650.3 (94.3)	973.4 (141.2)	1480.2 (214.7)	0.1422	24.9%	28.3%	33.3%	1038.7 (150.6)
133_5B2	5.050 (0.1988)	4.060 (0.1598)	5.000 (0.1969)	6.15 (0.2421)	1.905 (0.0750)	196.0 (28,426)	629.0 (91.2)	942.1 (136.6)	1421.7 (206.2)	0.1403	23.0%	35.4%	43.6%	1043.6 (151.4)
133_1C2	4.940 (0.1945)	3.910 (0.1539)	5.750 (0.2264)	7.50 (0.2953)	2.223 (0.0875)	191.0 (27,701)	626.8 (90.9)	944.4 (137.0)	1469.4 (213.1)	0.1489	30.4%	37.4%	46.8%	1096.1 (159.0)
Average Values						193.5 (28,064)	627.9 (91.1)	943.2 (136.8)	1445.5 (209.6)	0.1446	26.7%	36.4%	45.2%	1069.8 (155.2)

Table A-2: Summary of constant amplitude completely reversed fatigue test results for IT 131

Specimen ID	Test control mode	Test freq., Hz	E, GPa (ksi) [e]	At midlife ($N_{50\%}$)							$(2N_f)_{10\%}$, [b] reversals	$(2N_f)_{50\%}$, [c] reversals	Failure location [d]
				E', GPa (ksi)	$\Delta\varepsilon/2$, %	$\Delta\varepsilon_p/2$ (calculated), %	$\Delta\varepsilon_p/2$ (measured), %	$\Delta\sigma/2$, MPa (ksi)	σ_m, MPa (ksi)	$2N_{50\%}$, [a] reversals			
131_10	Strain	0.2	190.1 (27,571)	191.17 (27,726)	2.001%	1.538%	1.518%	892.81 (129.5)	-10.34 -(1.5)	128	-	246	IGL
131_8	Strain	0.25	191.74 (27,809)	182.63 (26,487)	2.008%	1.563%	1.520%	859.41 (124.6)	-10.87 -(1.6)	128	-	256	IGL
131_4	Strain	0.25	202.64 (29,390)	194.94 (28,273)	2.007%	1.532%	1.524%	916.6 (132.9)	-11.17 -(1.6)	128	-	292	IGL
131_9	Strain	0.4	194.74 (28,243)	187.39 (27,178)	0.999%	0.607%	0.583%	756.26 (109.7)	-7.881 -(1.1)	512	-	1,386	IGL
131_2	Strain	0.5	210.91 (30,589)	195.49 (28,352)	1.002%	0.587%	0.587%	801.75 (116.3)	-7.366 -(1.1)	512	-	1,432	IGL
131_12	Strain	0.5	197.89 (28,701)	191.74 (27,809)	0.993%	0.609%	0.591%	741.56 (107.6)	-8.609 -(1.2)	1,024	-	1,624	IGL
131_13	Strain	1	202.62 (29,386)	193.06 (28,001)	0.493%	0.156%	0.148%	650.14 (94.3)	3.0338 (0.4)	4,096	-	6,986	IGL
131_1	Strain	1	205.98 (29,874)	196.0 (28,423)	0.504%	0.162%	0.162%	659.7 (95.7)	-5.586 -(0.8)	4,096	-	8,338	IGL
131_5	Strain	1	187.93 (27,256)	188.6 (27,353)	0.500%	0.159%	0.140%	658.27 (95.5)	-2.785 -(0.4)	4,096	-	12,446	IGL
131_3	Strain	1.4	205.98 (29,873)	203.31 (29,487)	0.350%	0.042%	0.051%	594.0 (86.2)	29.193 (4.2)	16,384	-	23,820	IGL
131_15	Strain	1.4	183.84 (26,663)	201.93 (29,286)	0.350%	0.052%	0.050%	575.8 (83.5)	5.1724 (0.8)	32,768	-	50,088	IGL
131_16	Stain	1.4	189.8 (27,525)	197.7 (28,668)	0.350%	0.052%	0.046%	575.24 (83.4)	-36.21 -(5.3)	43,702	-	74,982	IGL
131_11	Load	15	-	-	0.250%	0.000%	-	499.68 (72.5)	0.9894 (0.1)	131,072	-	304,336	IGL
131_14	Load	15	-	-	0.250%	0.000%	-	499.49 (72.4)	1.5874 (0.2)	262,144	-	531,938	IGL
131_17	Load	15	-	-	0.250%	0.000%	-	499.84 (72.5)	1.2972 (0.2)	524,288	-	842,082	IGL
131_18	Load	20	-	-	0.200%	0.000%	-	399.97 (58.0)	0.8478 (0.1)	4,194,304	-	7,672,044	IGL
131_32	Load	20	-	-	0.200%	0.000%	-	390 (56.6)	0.5274 (0.1)	4,194,304	-	>10,000,000	No Failure
131_6	Load	20	-	-	0.175%	0.000%	-	337.66 (49.0)	0.9524 (0.1)	2,097,152	-	>10,000,000	No Failure

[a] $2N_{50\%}$ is defined as the midlife reversal

[b] $2(N_f)_{10\%}$ is defined as reversal of 10% max load drop

[c] $2(N_f)_{50\%}$ is defined as reversal of 50% max load drop

[d] IGL = Inside gage length; OGIT = Outside gage length but inside test section

[e] E value was calculated from the first cycle

Table A-3: Summary of constant amplitude completely reversed fatigue test results for IT 133

Specimen ID	Test control mode	Test freq., Hz	E, GPa (ksi) [e]	At midlife ($N_{50\%}$)							$(2N_f)_{10\%}$, [b] reversals	$(2N_f)_{50\%}$, [c] reversals	Failure location [d]
				E', GPa (ksi)	$\Delta\varepsilon/2$, %	$\Delta\varepsilon_p/2$ (calculated), %	$\Delta\varepsilon_p/2$ (measured), %	$\Delta\sigma/2$, MPa (ksi)	σ_m, MPa (ksi)	$2N_{50\%}$, [a] reversals			
133_4C1	Strain	0.3	188.44 (27,330)	182.6 (26,476)	1.995%	1.549%	1.506%	862.0 (125.0)	-7.1 -(1.0)	256	-	464	IGL
133_4B2	Strain	0.3	189.79 (27,526)	182.0 (26,397)	2.004%	1.560%	1.527%	857.2 (124.3)	-4.4 -(0.6)	256	-	498	IGL
133_3C2	Strain	0.5	209.26 (30,350)	196.7 (28,522)	1.001%	0.612%	0.604%	752.1 (109.1)	-6.5 -(0.9)	512	-	1,472	IGL
133_1B1	Strain	0.5	186.18 (27,002)	179.7 (26,068)	0.995%	0.622%	0.577%	721.2 (104.6)	-8.5 -(1.2)	1,024	-	2,124	IGL
133_7B1	Strain	1.0	184.74 (26,794)	179.2 (25,986)	0.501%	0.167%	0.143%	644.4 (93.5)	-10.4 -(1.5)	4,096	-	9,892	IGL
133_2D2	Strain	1.0	194.95 (28,274)	190.5 (27,624)	0.500%	0.166%	0.164%	647.6 (93.9)	1.1 (0.2)	4,096	-	10,732	IGL
133_6C2	Strain	1.0	187.28 (27,162)	189.1 (27,433)	0.499%	0.184%	0.167%	610.7 (88.6)	-8.4 -(1.2)	8,192	-	14,500	IGL
133_4D2	Strain	1.4	190.17 (27,580)	184.6 (26,770)	0.350%	0.059%	0.041%	562.9 (81.6)	-37.3 -(5.4)	16,384	-	28,556	IGL
133_4C2	Strain	1.4	198.75 (28,826)	204.8 (29,705)	0.349%	0.056%	0.065%	567.6 (82.3)	-5.0 -(0.7)	16,384	-	34,240	IGL
133_1B2	Strain	1.4	192.0 (27,850)	198.6 (28,797)	0.350%	0.059%	0.059%	563.3 (81.7)	-23.8 -(3.4)	16,384	-	44,334	IGL
133_1C1	Load	4.0	-	-	0.250%	0.013%	-	459.0 (66.6)	1.0 (0.1)	65,536	-	192,344	IGL
133_6B1	Load	4.0	-	-	0.250%	0.013%	-	458.2 (66.5)	1.3 (0.2)	131,072	-	255,404	IGL
133_1D2	Strain Load	2.0 3.0	197.56 (28,653)	204.6 (29,675)	0.250%	0.003%	0.013%	477.7 (69.3)	-97.6 -(14.2)	262,144	-	447,542	IGL
133_1D1	Load	25.0	-	-	0.200%	0.000%	-	389.8 (56.5)	1.6 (0.2)	524,288	-	1,078,788	IGL
133_7C1	Load	25.0	-	-	0.200%	0.000%	-	389.4 (56.5)	0.1 (0.0)	1,048,576	-	1,736,708	IGL
133_3B2	Load	25.0	-	-	0.200%	0.000%	-	389.9 (56.5)	0.9 (0.1)	1,048,576	-	2,142,424	IGL
133_2C1	Load	25.0	-	-	0.175%	0.000%	-	338.3 (49.1)	0.2 (0.0)	2,097,152	-	>10,000,000	No Failure
133_3B1	Load	25.0	-	-	0.175%	0.000%	-	336.2 (48.8)	-0.3 (0.0)	2,097,152	-	>10,000,000	No Failure

[a] $2N_{50\%}$ is defined as the midlife reversal

[b] $2(N_f)_{10\%}$ is defined as reversal of 10% max load drop

[c] $2(N_f)_{50\%}$ is defined as reversal of 50% max load drop

[d] IGL = Inside gage length; OGIT = Outside gage length but inside test section

[e] E value was calculated from the first cycle

Table A-4 : Summary of the periodic overload fatigue test results for IT 131/132

Spec. ID	Test Control Mode [c]	Test Freq. OL/SC (Hz)	Load history Description												Exp. Life (Blks)	$N_{f,\,sc(eq)}$ (Cycles)	OL Damage Ratio	Failure Location [a]
			$\varepsilon_{a,\,SC}$ (%)	$\varepsilon_{m,\,SC}$ (%)	$\Delta\varepsilon_p/2_{,\,SC}$ (calculated) (%)	$\sigma_{a,\,SC}$ (MPa) [b]	$\sigma_{m,\,SC}$ (MPa) [b]	N_{SC} (Cycles)	$\varepsilon_{a,\,OL}$ (%)	$\Delta\varepsilon_p/2_{,\,OL}$ (calculated) (%)	$\sigma_{a,\,OL}$ (MPa) [b]	$\sigma_{m,\,OL}$ (MPa) [b]	$N_{f,\,OL}$ (Cycles)					
132_23	Load	1.3 / 4	0.200%	0.200%	0.003%	385.8	228.5	40	0.399%	0.085%	615.4	0.0	10,000	484	22,734	0.148	IGL
132_20	Load	1.3 / 4	0.200%	0.200%	0.003%	385.8	228.4	40	0.399%	0.085%	615.4	0.0	10,000	720	34,783	0.172	IGL
132_31	Load	1.3 / 30	0.200%	0.200%	0.003%	385.7	228.5	40	0.399%	0.085%	615.3	0.0	10,000	724	34,993	0.172	IGL
132_21	Load	1.3 / 4	0.125%	0.275%	0.000%	244.0	370.3	100	0.399%	0.085%	615.4	0.0	10,000	686	82,511	0.169	IGL
132_29	Load	1.3 / 4	0.125%	0.275%	0.000%	244.1	370.2	150	0.399%	0.085%	615.5	0.0	10,000	695	125,527	0.170	IGL
132_25	Load	1.3 / 4	0.125%	0.275%	0.000%	244.1	370.3	100	0.399%	0.085%	615.4	0.0	10,000	2,138	311,571	0.314	IGL
132_24	Load	1.3 / 12	0.100%	0.300%	0.000%	195.2	419.2	300	0.399%	0.085%	615.4	0.0	10,000	649	233,146	0.165	IGL
132_22	Load	1.3 / 4	0.100%	0.300%	0.000%	195.2	419.2	200	0.399%	0.085%	615.4	0.0	10,000	1,744	480,706	0.274	IGL
132_28	Load	1.3 / 30	0.075%	0.324%	0.000%	146.3	468.3	2,000	0.399%	0.085%	615.4	0.0	10,000	397	922,934	0.140	IGL
132_30	Load	1.3 / 12	0.075%	0.324%	0.000%	146.4	468.3	2,000	0.399%	0.085%	615.5	0.0	10,000	513	1,208,908	0.151	IGL

[a] IGL = Inside gage length

[b] All stress values reported are from mid-life

[c] Load-controlled tests were pre-cycled at the OL strain amplitude of 0.50% for 1000 cycles. Damage from the pre-strained cycles is included in the OL damage ratio

Table A-5 : Summary of the periodic overload fatigue test results for IT 133/134

Spec. ID	Test Control Mode [c]	Test Freq. OL/SC (Hz)	Load history Description												Exp. Life (Blks)	$N_{f,\,sc(eq)}$ (Cycles)	OL Damage Ratio	Failure Location [a]
			$\varepsilon_{a,\,SC}$ (%)	$\varepsilon_{m,\,SC}$ (%)	$\Delta\varepsilon_p/2_{,\,SC}$ (calculated) (%)	$\sigma_{a,\,SC}$ (MPa) [b]	$\sigma_{m,\,SC}$ (MPa) [b]	N_{SC} (Cycles)	$\varepsilon_{a,\,OL}$ (%)	$\Delta\varepsilon_p/2_{,\,OL}$ (calculated) (%)	$\sigma_{a,\,OL}$ (MPa) [b]	$\sigma_{m,\,OL}$ (MPa) [b]	$N_{f,\,OL}$ (Cycles)					
134_4D1	Load	1.3 / 4	0.175%	0.225%	0.001%	335.6	260.6	40	0.399%	0.090%	597.4	0.0	10,000	877	43,186	0.188	IGL
134_7B2	Load	1.3 / 4	0.175%	0.225%	0.001%	335.6	260.6	40	0.399%	0.090%	597.4	0.0	10,000	1,561	83,936	0.256	IGL
134_2B1	Load	1.3 / 4	0.125%	0.275%	0.000%	240.3	356.0	80	0.399%	0.090%	597.4	0.0	10,000	376	34,879	0.138	IGL
134_6C1	Load	1.3 / 4	0.125%	0.275%	0.000%	240.3	355.9	80	0.399%	0.090%	597.4	0.0	10,000	592	56,327	0.159	IGL
134_7D2	Load	1.3 / 4	0.090%	0.310%	0.000%	173.1	423.3	160	0.399%	0.090%	597.4	0.0	10,000	1,117	226,716	0.212	IGL
134_2B2	Load	1.3 / 4	0.090%	0.310%	0.000%	173.2	423.3	160	0.399%	0.090%	597.4	0.0	10,000	1,758	388,401	0.276	IGL
134_3C1	Load	1.3 / 12	0.070%	0.329%	0.000%	135.1	461.5	1,200	0.399%	0.090%	597.4	0.0	10,000	321	443,830	0.132	IGL
134_3D2	Load	1.3 / 12	0.070%	0.329%	0.000%	135.1	461.5	1,200	0.399%	0.090%	597.4	0.0	10,000	1,145	1,749,204	0.215	IGL
134_5C2	Load	1.3 / 30	0.060%	0.339%	0.000%	115.1	481.7	2,000	0.399%	0.090%	597.4	0.0	10,000	1,146	2,918,258	0.215	IGL
134_5D1	Load	1.3 / 30	0.060%	0.339%	0.000%	115.0	481.6	2,000	0.399%	0.090%	597.4	0.0	10,000	1,284	3,328,149	0.228	IGL

[a] IGL = Inside gage length

[b] All stress values reported are from mid-life

[c] Load-controlled tests were pre-cycled at the OL strain amplitude of 0.50% for 1000 cycles. Damage from the pre-strained cycles is included in the OL damage ratio

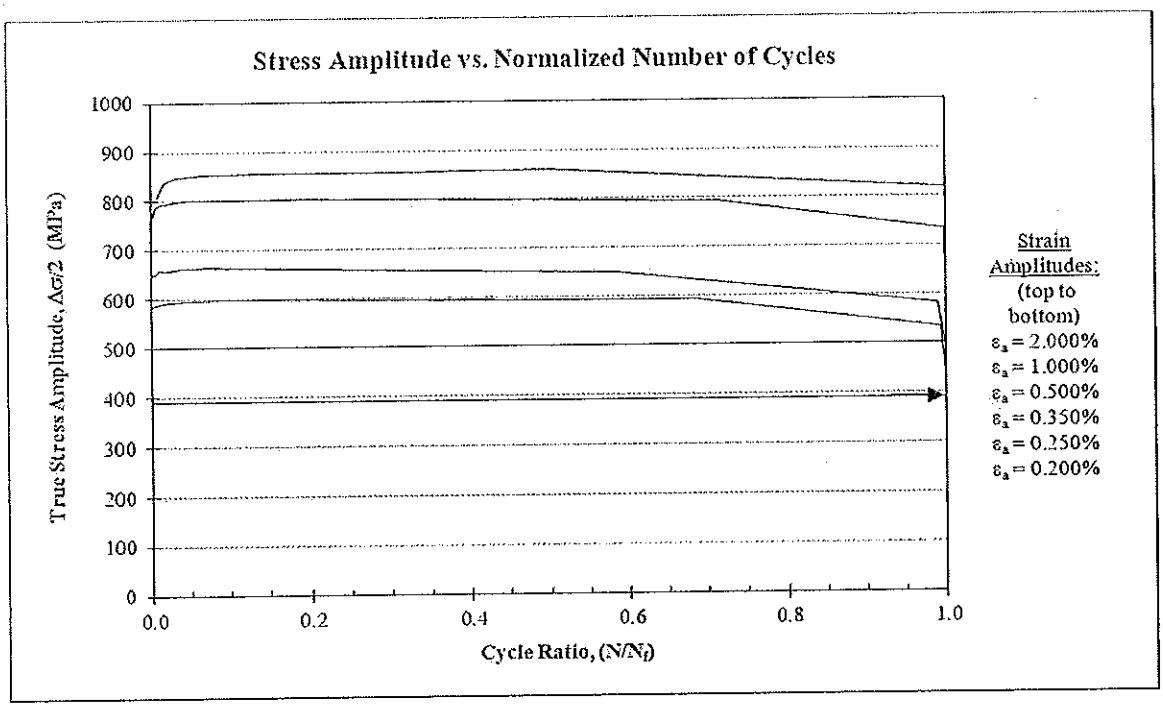

(a)

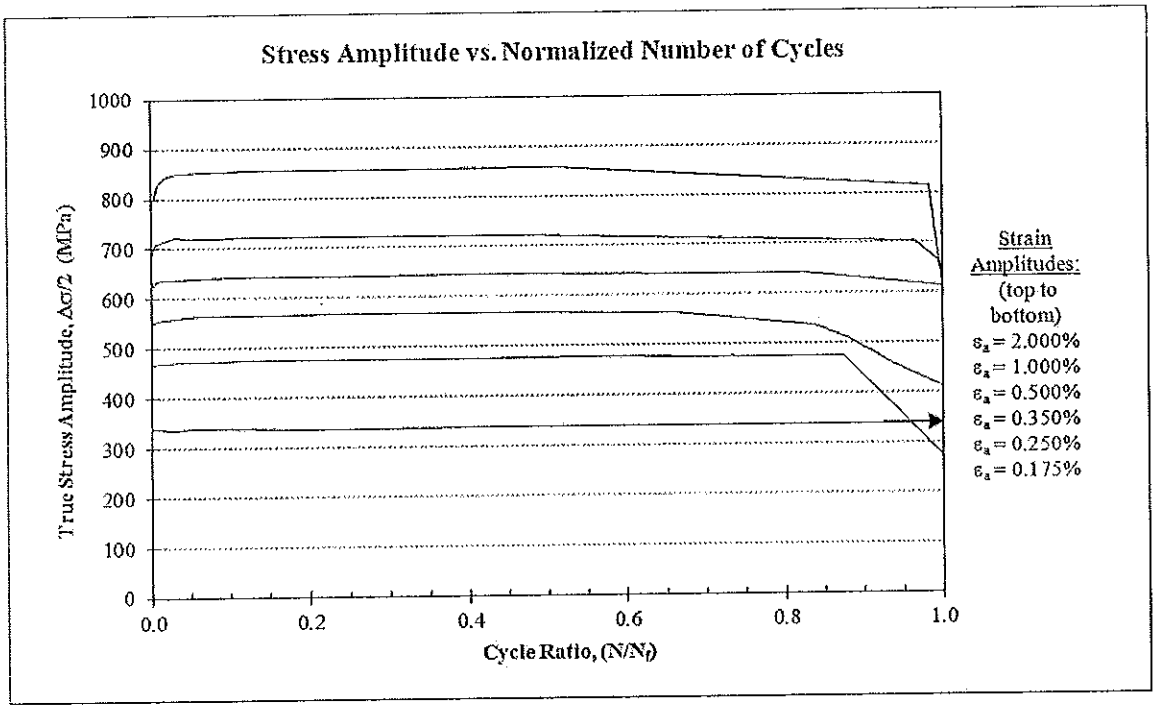

(b)

Figure A-1: True stress amplitude versus normalized number of cycles for (a) IT 131 and (b) IT 133

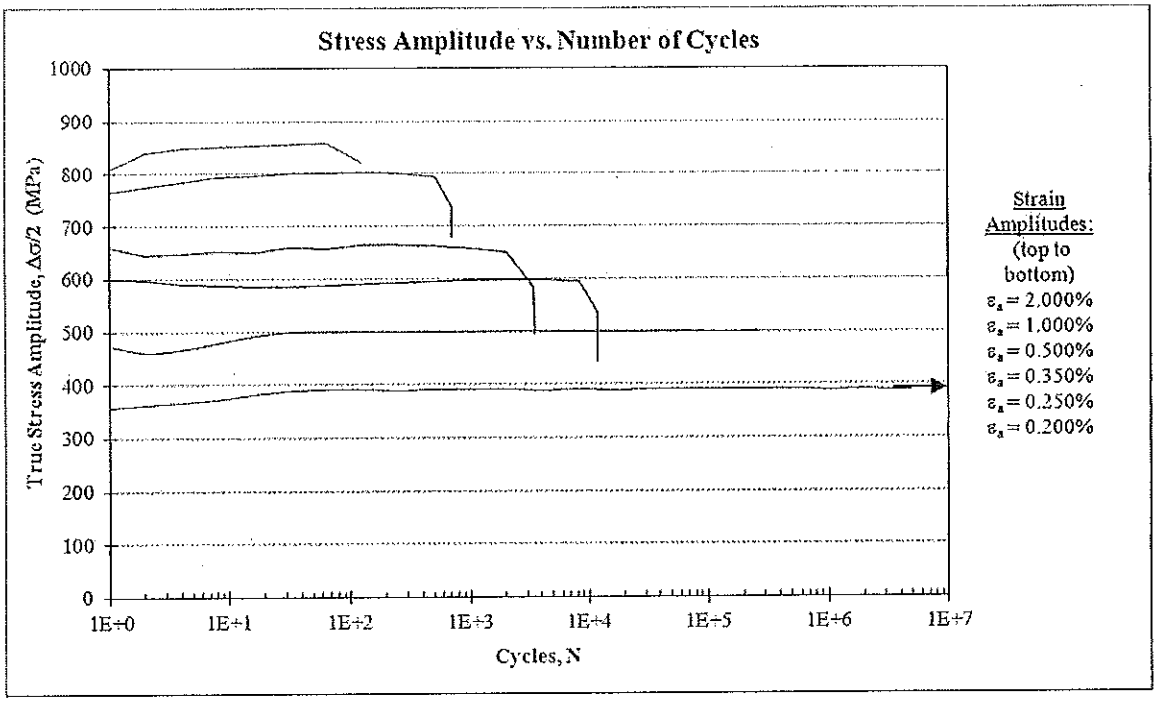

(a)

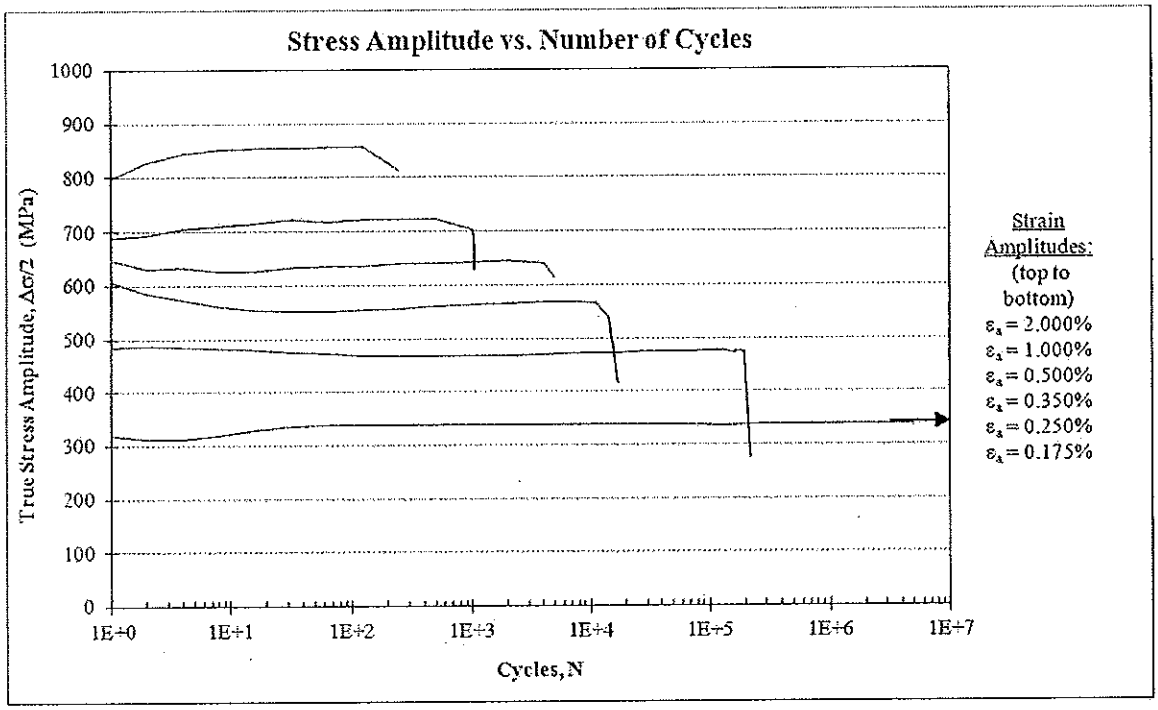

(b)

Figure A-2: True stress amplitude versus number of cycles for (a) IT 131 and (b) IT 133

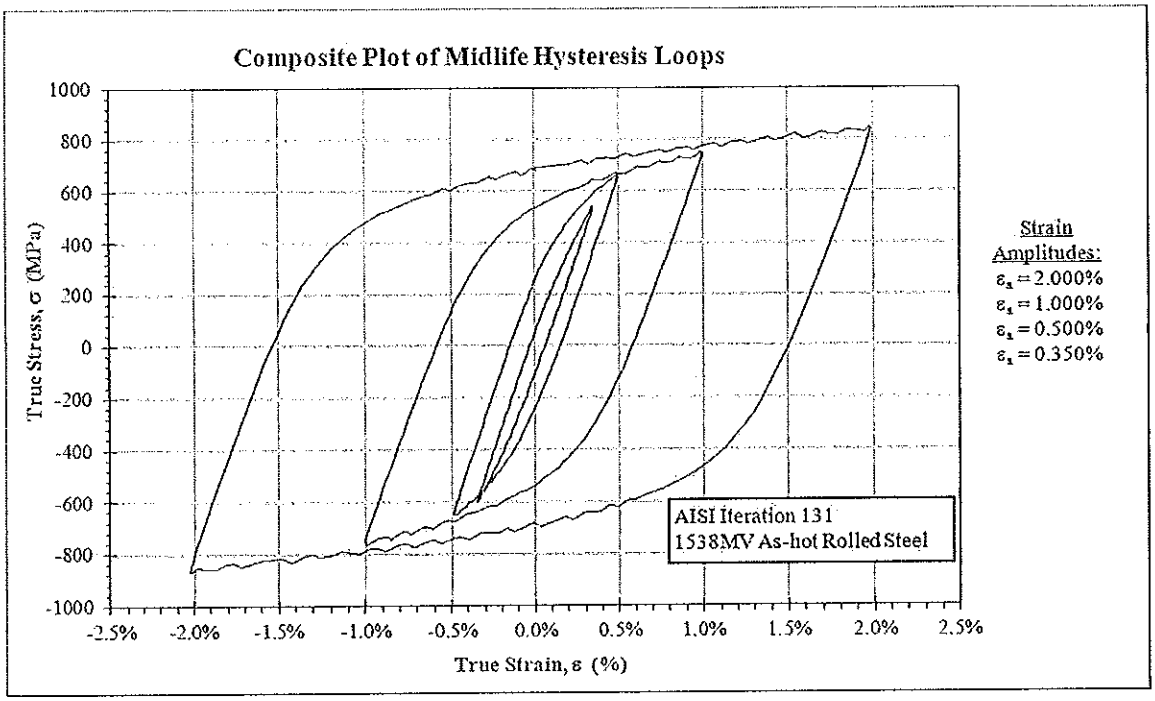

(a)

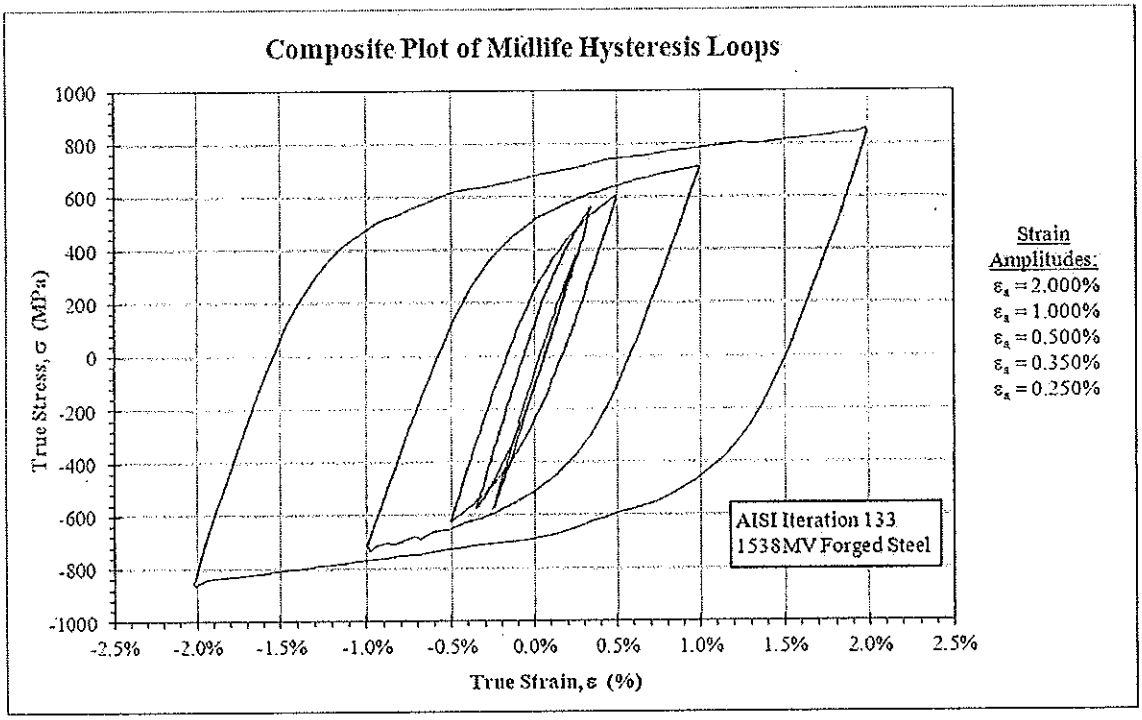

(b)

Figure A-3: Composite plot of midlife hysteresis loops for (a) IT 131 and (b) IT 133